IPTC 11968

Comprehensive Mini-Frac Testing in the Gullfaks Field as a Tool for Characterization of Reservoir Structure and Rock Mechanics.

Arthur Bale, StatoilHydro, SPE, Haakon Fossen, University of Bergen, Eirik Berg, StatoilHydro, SPE, Øystein Mjelde, StatoilHydro, SPE, Trond Kui, StatoilHydro, SPE.

This paper was prepared for presentation at the International Petroleum Technology Conference held in Kuala Lumpur, Malaysia, 3–5 December 2008.

Abstract

This paper describes the stress field and rock mechanical aspects in the Gullfaks Field reservoirs. The data analyses are mainly based on large volume water and gel "mini-fracs" associated with data gathering in conjunction with propped fracture stimulation jobs. A few data points represent results from Pump-In/Decline Tests after perforating/before start-up of single zone water injectors. The data are based on "state of the art" mini-frac analysis techniques which also are discussed in this paper.

The tests have been carried out over a 20 year period with varying or cycled reservoir pressure. The systematized data from 52 mini-frac tests executed in sandstone with high porosity, high permeability and very low effective stresses give results that cohere with linear elastic rock mechanical theory. The connection between faults, tectonics and local stress is discussed. The data represent a unique gathering of information which has supplemented to the understanding of the overall geological structural picture. Further, this paper discusses how the analysis of data founded a revised approach to solve drilling challenges as a result of small drilling margins and localized depletion. Also, this paper presents a new graphical solution illustrating the depletion dependant stress change versus reservoir configuration or structural boundaries.

Introduction

The Gullfaks Field is located in the central part of the East Shetland Basin in the Northern North Sea. The StatoilHydro operated field has been developed with 3 Condeep platforms and started production (Phase-1 Development from GFA and GFB) in December 1986. Production from GFC (Phase-2 Development) commenced in Janauary 1990. A total of 188 development wells (including all side tracks and 6 subsea wells) have been drilled as of December 2007. Field peak production was exceeding 95,000 Sm^3/d (≈ 600,000 bopd) in 1994. Current production averages 16,000 Sm^3/d (100,000 bopd). Predicted ultimate oil production from the field is more than 358 Mill Sm^3 (2,252 Mill bbl), of which 335 Mill Sm^3 (2,107 Mill bbl) had been produced by January 1st 2008. Forecasted ultimate oil production from the field represents 62 percent field recovery.

The main drive mechanism is water injection with some scattered and intermittent gas injection in mainly downflank WAG injectors.

The oil is mainly located within three major sandstone units, the Middle Jurassic Brent Group and the Early Jurassic Statfjord and Cook Formations, containing approximately 75 percent, 16,5 percent and 7,5 percent, respectively, of the mapped hydrocarbon pore volume (STOOIP) of 582 million Sm^3 (3,660 million bbl) in place. The Lower Brent delta sequence is comprised of the Broom/Rannoch, Etive and Ness Formations, and the Upper Brent consists of the Tarbert Formation. Broom/Rannoch/Etive, Ness and Tarbert are considered as three separate reservoirs with regard to field development.

The reservoirs are highly overpressured, with a representative initial reservoir pressure of 310 bar (4,495 psi) at datum depth (1850 m (6070 ft) below mean sea level). Reservoir temperature is 72 deg. C (162 deg. F) at datum level. The shallow, highly porous and permeable sands, consisting of mainly quartz, feldspars together with autogenious kaolinite, mica and calcite filling, are generally poorly consolidated. Net-pay porosity and permeability vary between 28-38 percent and 2.0 - 10,000 md, respectively. The oil is undersaturated, with a typical saturation pressure of approximately 245 bar (3550 psi), depending on formation, depth and location.

Production wells in the Rannoch and Cook Formation are mainly IVFC (indirect vertical fracture completion) wells. These wells are propped fracture stimulated through perforations/completions in lower stratigraphical zones with lower permeability and higher sand strength which communicate with overlying high permeability and weak zones through the propped fracture[1, 2]. The majority of stress test data published in this paper results from mini frac analyses in conjunction with these stimulation jobs.

Information regarding formation minimum principal stress is not crucial information limited to design of propped fracture stimulation jobs; characterization of formation stress also represents mandatory or important information in conjunction with

1. formation strength, formation collapse and kill calculations in conjunction with well planning,
2. sand prediction work,
3. reservoir compaction and subsidence calculations,
4. design of surface water injection equipment,
5. choice of perforation strategy in wells with multiple injection zones,
6. matrix scale squeeze and stimulation operations,
7. calculation of thermo-elastic effects due to reservoir cooling, and, as shown in this paper,
8. characterization of reservoir structure or fault placements.

Gullfaks Field Structure Development

Structurally, the Gullfaks Field is located in the eastern part of a 10-25 km wide first-order fault block in the North Sea rift system, **Fig. 1**. A large amount of seismic 3D data,

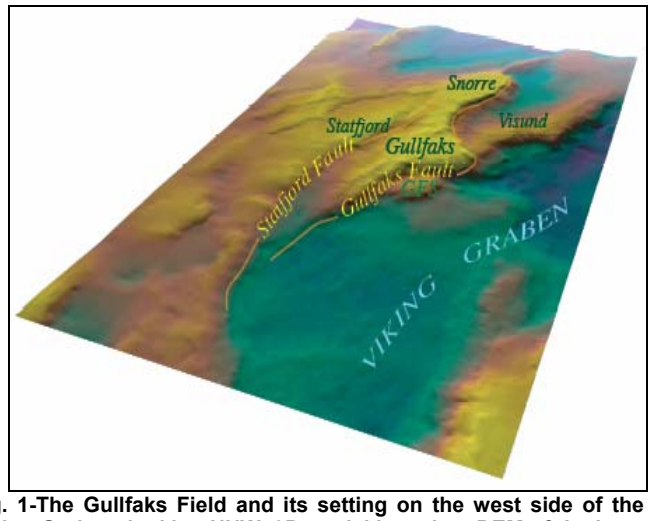

Fig. 1-The Gullfaks Field and its setting on the west side of the Viking Graben, looking NNW. 3D model based on DEM of the base Cretaceous surface.

core data, dipmeter data and other well log data from close to 150 km drilled reservoir have provided the basis for the current picture of the severely faulted Gullfaks reservoirs[3].

The Gullfaks Field is divided into three structural domains, **Fig. 2**. The largest domain is a domino-style fault system with easterly dipping faults and westerly dipping bedding separated from a deeply eroded eastern horst complex of elevated subhorizontal layers and steep faults by a transitional zone graben system. Most of the reservoir volume is located within the domino system, where the main faults (100-300 m throw) trend N-S and dip 25-30° to the east. Minor faults in this area show a considerable variation in orientation and are mainly the results of local adjustments within the main N-S oriented fault blocks in the field.

It has, based on deep seismic data, been suggested that a low-angle detachment fault underlies the Gullfaks Field reservoirs[4]. If present, such a detachment is expected to have formed as a response to gravitational instability after the main

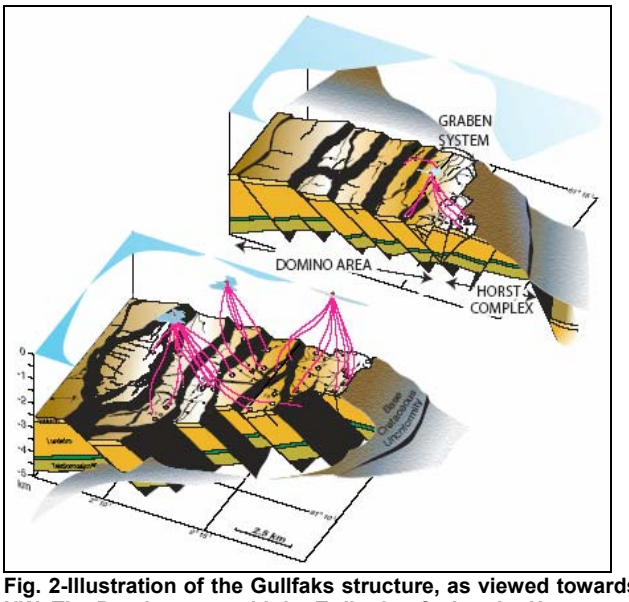

Fig. 2-Illustration of the Gullfaks structure, as viewed towards the NW. The Domino area with its E-dipping faults, the Horst complex and the transitional Graben system are shown, as are the three platforms with some of their reservoir wells.

fault pattern of the field had been established and after the field was established as a positive structure in the late Jurassic.

The northern North Sea is influenced by at least two main phases of post-Devonian extension. The first of these is a Permo-Triassic stretching phase during which the northern North Sea was established as a rift zone. Many of the major faults, such as the Statfjord and Gullfaks faults, were established during this phase. After a rather quiescent period, stretching commenced during deposition of the uppermost part of the Brent Group, i.e. in the late Middle Jurassic and lasted until the earliest Cretaceous. The faults in the Gullfaks reservoirs all formed during this phase.

The late Jurassic deformation of the field was extensional, and map-view restoration indicates approximately plane strain with extension in the E-W direction[5], **Fig. 3**. Total Jurassic-Cretaceous E-W extension is estimated to ~40%, with a

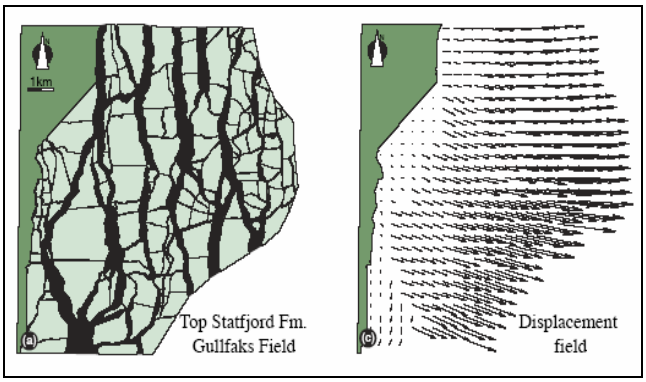

Fig. 3–Map of the top Statfjord Formation of the Gullfaks Field and the displacement field that emerge from fault block reconstruction, i.e. by closing the gaps between fault blocks. Modified from Rouby et al. (1996).

somewhat higher percentage in the domino area and a lower percentage in the horst complex. Although a (W)NW-(E)SE extension direction has been suggested for the Northern North Sea[6], the Gullfaks strain data, fault orientation and fault geometry analyses[3] are consistent with the general view that the Jurassic-Cretaceous extension was oriented closer to E-W in this part of the North Sea. Hence, a regional late Jurassic-early Cretaceous stress field with an E-W oriented minimum horizontal stress may be inferred.

Gullfaks was a structural high throughout most of the Cretaceous, but was submerged and covered by sediments in the late Cretaceous. Minor reactivation of some of the main faults within the field and the Gullfaks Fault to the east is at least partly related to differential compaction rather than tectonic stress. E-W oriented extensional faults of Tertiary age are mapped in the Snorre area to the north, **Fig. 1**, probably linked to the opening of the Atlantic Ocean at that time. Their presence may indicate a more N-S oriented minimum horizontal stress direction for at least part of the Tertiary period.

Studies[7, 8] of current stress dirctions in the northern North Sea show maximum horizontal stress in the Gullfaks area to be approximately perpendicular to the Viking Graben (+/- 110 degrees from north). The present stress picture is probably controlled by plate tectonic stresses set forth by the North Atlantic Ridge push.

Field Example and Mini-frac Analysis Procedure

The stress data presented in this paper are solely based on results from "large scale" (large volume and high rate) Pump-In/Decline Tests using water or gel. Thus, no data points are based on Leak-off Tests (LOT) or extended Leak-off Tests (X-LOT) typically executed in conjunction with drilling operations. Pump-In/Flowback Tests have not been undertaken in this field because such tests would be extremely difficult to operate due to the relatively high fluid loss typically encountered. Large scale mini-frac testing probably represents the most reliable stress testing procedure because,

1. this type of testing is not (or less) vulnerable to poor cement jobs which may complicate analysis of small volume and low rate injection tests,
2. high rates "assure" fracturing of the formation or sq. rt of time related ("Carter") leak-off, increases "fluid-efficiency" and thus "time to fracture closure". Also, large volumes allow extended time between shut-in and fracture closure which in turn simplifies the pressure transient analysis of the decline data,
3. large volume fracturing (typically a half string volume) allows mandatory diagonostics of all pressure transient periods associated with pressure decline of a closing fracture.

The mini-frac stress test data presented in this paper are consistently extracted from Pump-In/Decline Tests, **Fig. 4,** where pump rates on the order of 30 - 40 bpm (4,770 – 6,360 lpm) represent typical values for constant rates during injection. Pump times in conjunction with water injection are limited to (dependant on permeability) typical 10 minutes in order to maintain "Carter Leak-off" during injection. Pump rates have always been kept constant in order to simplify the pressure transient analysis of the pressure decline data. Shut-in of injection has always been "instant" in order to diagnose instantaneous shut in pressure (ISIP) and perforation friction. The results from the Pump-In/Decline Tests have most often been "supported" by a Step-Rate Test (SRT) before or after the Pump-In/Decline Tests.

The analysis procedure of large scale Pump-In/Decline Test data normally consists of recognizing four time periods or pressure ranges, as pictured in **Fig. 4,** of which the two earliest phases are "matched" by use of sophisticated Pseudo 3-D or "true" planar 3-D Frac Models which fully couple fluid flow with rock mechanics. These types of models require comprehensive in-put of reservoir, mini-frac fluid and rock mechanical data. First, 3 shut-in pressure decline periods (Phase I, Phase II and Phase III) must be identified, **Fig. 4**:

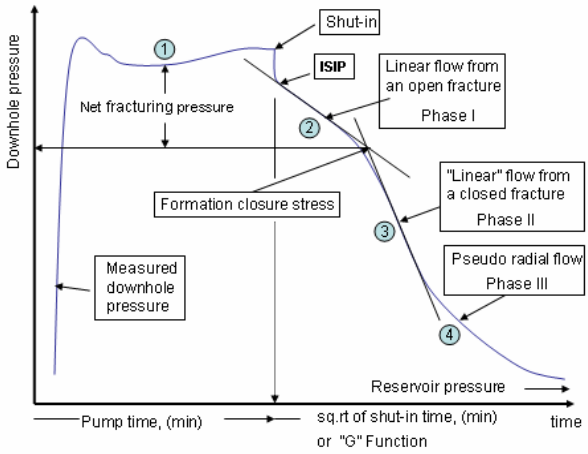

Fig. 4–Illustrative Pump-In/Decline Test Analysis

1. "linear" flow perpendicular to fracture azimuth from an open, propagating and closing/receding fracture (Phase-I), followed by
2. "linear" flow perpendicular to fracture azimuth from a closed fracture towards undisturbed reservoir pressure caused by still large pressure differential between the closed fracture and undisturbed or original reservoir pressure (Phase II)– and finally
3. pseudo-radial dominated flow (Phase III) most often observed at downhole wellbore pressures significantly below fracture closure pressure (minimum principal horizontal stress).

Note that all three flow regimes or "Phases" above are typically present in large volume injection/decline tests in moderate to high permeability formations. However, under other conditions, one or more of the flow regimes may not be present. That is, for very high permeability, the flow behavior may transition directly from Phase I to Phase III, or for low permeability, unless shut-in time is very long, the flow behavior may not reach Phase III, etc.

The analysis procedure for any stress test program should first be to "frame" the closure stress. "Fracture extension pressure" from SRT gives an upper bound for closure pressure or

formation minimum principal stress. This parameter typically exhibits values (slightly dependant on well deviation and azimuth) on the order of 15-25 bar (217-362 psi) above fracture closure pressure in the unconsolidated Gullfaks reservoir zones if the SRT test is undertaken before the gel mini-frac, **Fig. 5**. Thus, a fracture extension pressure of 357.6 bar in **Fig. 5** indicates minimum principal stress to be between 332.6 bar and 342.6 bar (4823 – 4968 psi) in Gullfaks well C-42T3 which represents the stress test field example in this paper. ISIP after the gel mini-frac injection typically exceeds fracture closure stress in Gullfaks by 10-15 bar (145-217.5 psi) and thus represents an even closer upper bound value for closure stress.

In case of constant injection rate, initiation of pseudo-radial flow, **Figs. 4 and 6**, can be picked by using a Horner Plot for the shut-in decline data for the Pump-in/Decline Test. Thus, a lower bound for the closure stress can be picked. Defining start of pseudo-radial flow is generally very important; often this deflection point on a sq.rt of time ($\sqrt{t_s}$) plot is presented as an erroneous interpretation of formation closure stress. The net result will be far too high net (fracturing) pressure, **Fig. 4**, (nearly always explained by multiple fractures or near wellbore tortuosity) and far too high values for "fluid- efficiency" which finally will occasion pre-mature screenouts during the subsequent fracture stimulation jobs since the erroneous interpretation of high fluid efficiency will lead to pumping an inadequate pad volume.

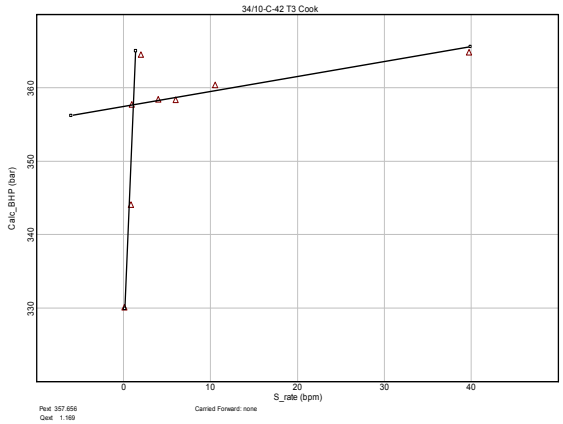

Fig. 5–SRT with slick water prior to gel mini-frac in Gullfaks Well C-42T3

Fig. 6 shows start of pseudo-radial flow at about 327 bar (4742 psi); hence, this pressure represents a lower bound for closure stress in Well C-42T3. Although ISIP and start of pseudo-radial flow represent an upper and lower bound, respectively, for closure stress, one should realize that these values may be several 10's of bar above and below fracture closure pressure for stiff rock.

The pressure decline rate, $\Delta P/\Delta\sqrt{t_s}$, for the Phase I time period, which is dominated by fracture storage parameters, can be represented by the relation

$$\frac{\Delta P}{\Delta\sqrt{t_s}} \propto \frac{C_L H_p E}{H^2} \qquad \ldots\ldots\ldots\ldots\ldots\ldots\ldots\ldots (1)$$

The $\sqrt{t_s}$-plot is used because the rate of pressure decline before the fracture closes is proportional to fluid loss

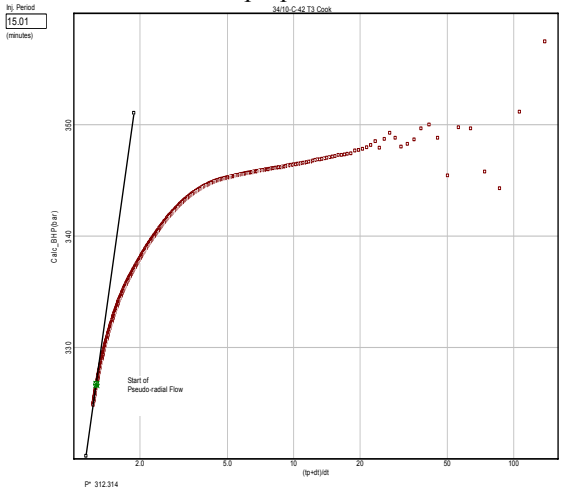

Fig. 6–Horner Plot for gel mini-frac in Gullfaks Well C-42T3

from the fracture. Since (Carter) fluid loss, **Eq. 2**, depends on the sq. rt of time, it follows that pressure decline should

$$v_L = \frac{C_L}{\sqrt{t}} \qquad \ldots\ldots\ldots\ldots\ldots\ldots\ldots\ldots (2)$$

depend on the sq. rt of time (or $\sqrt{t_s}$). Theoretically, this dependence is not linear; that is no straight line should be expected because the time reference (i.e., when the fracture opened) is variable along the length of the fracture. However, experience indicates that approximately straight lines occur indicating that fluid loss at the fracture tip often dominates the behaviour.

The pressure decline rate for Phase II, which is governed by formation "diffusivity", can be represented by

$$\frac{\Delta P}{\Delta\sqrt{t}} \propto \frac{k}{\phi\mu C_t X_f^{\,2}} \qquad \ldots\ldots\ldots\ldots\ldots\ldots\ldots\ldots (3)$$

The pressure decline rate for Phase I will, as discussed above, plot as a straight line versus sq.rt of shut-in time, $\sqrt{t_s}$. The point where the fracture closes should cause a drastic change in the flow system or total system compressibility and a distinct change in slope on the $\sqrt{t_s}$-plot. However, the change in slope may be either "up" or "down", depending on the relative relationship of the fracture's variables and those of the reservoir, as specified in **Eqs. 1 a**nd **3**. This implies a theoretical possibility that no change in slope may occur. Experience from this type of stress testing in Gullfaks, however, proves that pumping two different volumes or a different type of injection fluid (water or gel) will normally solve that problem. The steeper slope for Phase II in **Fig. 4** is typical for formations with large transmissibility (Kh/μ) or large formation diffusivities as typically encountered in gas reservoirs or high permeability oil bearing formations as found in the Gullfaks Field. However, for the field case presented in this paper, the $\sqrt{t_s}$-plot for the gel mini frac, **Fig. 7**, reveals two possible fracture closure pressures of 344.5 bar and 338.3 bar, respectively. This "complicated" example is enclosed to show

that determination of fracture closure pressure sometimes might not be "straight forward" – even for simple reservoirs as typically found in the Gullfaks Field. Anyhow, the early and high value of 344.5 bar can be ignored in this case because of unrealistic appurtenant leak-off coeffisients and far too low net-pressures for this formation. Also, the early deflection point in this case is plausibly attributed to extensive fracture height growth into the lesser depleted zone above the perforation interval. When pumping stopped, the high stress zone closed first, forcing fluid back into the "main" fracture and thus created a relatively slow, flat pressure decline. The early and slow pressure decline rate during the first five

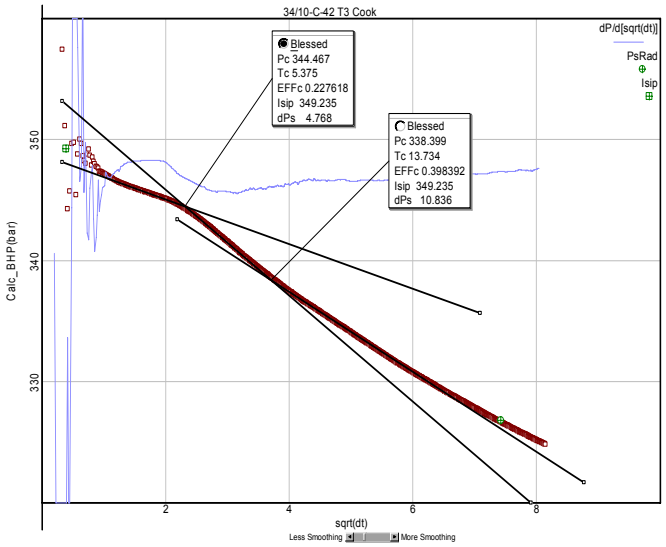

Fig. 7–Sq. rt of time ($\sqrt{t_s}$) plot of gel mini-frac in Gullfaks Well C-42T3 revealing false and true fracture closure pressures

minutes of the shut-in is therefore caused by combined redistribution of frac fluid towards the injection zone (pressure maintenance) and height recession during the closing period of the fracture; the rapid pressure decline below 344.5 bar (the real Phase I period in **Fig. 4**) is due to reduced height and thus a "stiffer" formation since fracture compressibility is related to the identity

$$C_f \approx \frac{2}{\pi}\frac{E}{\overline{P_{net}}H^2 L}\frac{Q_L \Delta t}{\Delta P_{net}} \quad \ldots\ldots\ldots\ldots\ldots\ldots\ldots\ldots (4)$$

The slower pressure decline rate after closure in this case is explained by an unusual low permeability (on the order of 1 md) in the execution zone.

Another option would be to plot the pressure shut-in data versus the "G"-Function, **Fig. 8**. This function is essentially a superposition sq.rt time function that accounts for the variations in fluid loss time along the fracture length. The "G"-Function is found to work better for high fluid loss cases where closure time is on the order of 20 to 30 percent of pump time or less[9]. Experience from Gullfaks confirms the validy of this method for low "fluid-efficiency" fracturing cases. Note that for the $\sqrt{t_s}$-plot, the slope of the pressure vs. time during Phase I behavior is proportional to several fracture variables, **Eq. 1**. However, on the 'G' Plot, the slope of the Pressure vs. 'G' line during Phase I is EQUAL to these variables,

$$\frac{\Delta P}{\Delta G} = -\frac{C_L H_p E \sqrt{T_P}}{H^2} = -\Delta P^* \quad \ldots\ldots\ldots\ldots\ldots\ldots (5)$$

and this collection of variables is given a label – ΔP*. If ΔP* is measured from the 'G' Plot, and if height, "H", and modulus, "E", are known, the fluid loss coefficient, "C_L", can be determined. Note that the particular form of ΔP* above is for a confined height fracture, and the relation is slightly different for radial fracture geometry.

Interestingly, in addition to picking formation closure stress, the false closure pressure in this field example can be used to calculate the stress differential between the execution zone and adjacent strata by use of the "G"-Function plot. The equations

$$\Delta\sigma_x = \Delta P / 0.4 \quad \ldots\ldots\ldots\ldots\ldots\ldots\ldots\ldots\ldots\ldots (6)$$

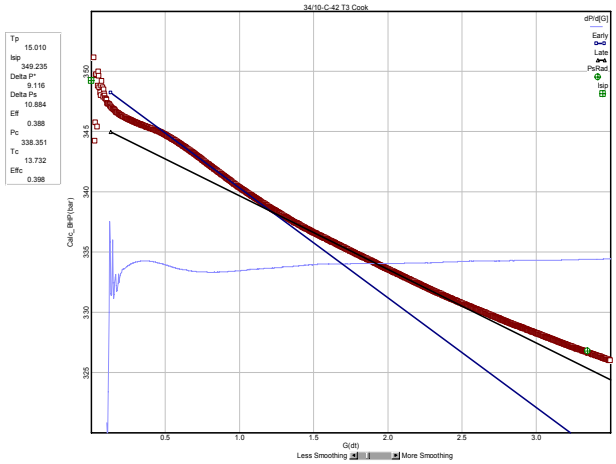

Fig. 8–G(dT) plot of gel mini-frac in Gullfaks Well C-42T3

and

$$\Delta P_s = 0.8\Delta\sigma_x \quad \ldots\ldots\ldots\ldots\ldots\ldots\ldots\ldots\ldots\ldots (7)$$

with reference to **Fig. 9**[10], give nearly identical result, 15.2 bar and 13.5 bar, respectively, with respect to stress differential.

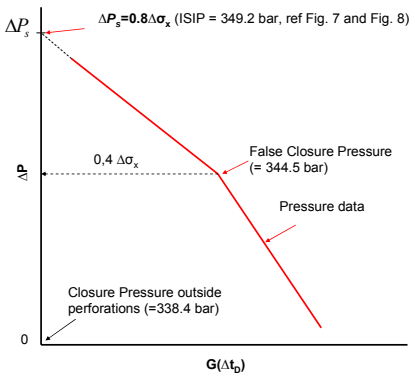

Fig. 9–G(dT) plot of gel mini-frac in Gullfaks Well C-42T3

Eq. 6 is most appropriate in this case since it relates to a viscous (Newtonian) fluid. This stress differential was an import input to the design of the successful main fracture stimulation job in well C-42T3.

A Log-Log Plot, **Fig. 10**, of the pressure derivative of the pressure decline data may sometimes clarify the analysis of "hard" data. Ideally, the pressure derivative behaviour of the post wellbore storage decline data should (after wellbore storage) chronologically plot as a half-slope, unit-slope and, finally, a half-slope. The first half-slope represents linear flow from an open and still propagating fracture after shut-in (post shut-in extension or afterflow). While this phase may be extensive for a typical Perkins & Kern type fracture

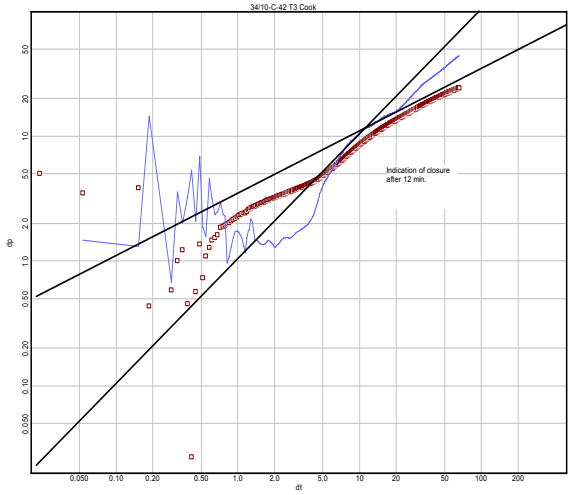

Fig. 10–Log-log Plot of gel mini-frac in Gullfaks Well C-42T3

(length >> height) it will be of minor importance for a radial fracture. This time period comes under the early part of Phase I in **Fig. 4.** The unit-slope, which represents (changing) fracture storage due to length or height recession corresponds to the last part of Phase I in **Fig. 4**. The final half-slope represents formation "linear" flow from a closed fracture (Phase II) before the curve flattens out on the log-log plot due to (pseudo) radial flow. These pressure trends are hard to identify in **Fig. 10**, and this diagonostic technique has not proven to be helpful in conjunction with mini frac analysis in the Gullfaks Field due to approximate radial fracture configurations in most cases.

Sometimes, the G-dP/dG-Plot[11] may give valuable information. This method has proven to be a valuable diagonostic in order to identify natural fractures and/or excessive height growth. This technique has not contributed to clarification of complex data gathered from the high fluid-loss environment encountered in Gullfaks, although the result from this technique substantiates the conclusion from the standard methods in case of the subject field example, **Fig. 11**. For high fluid loss cases, this plot is often less reliable. Basically, the information of interest is the slopes and slope changes (i.e., the derivative). This plot takes the derivative and multiples this by a small value of 'G' – since for high fluid loss cases fracture closure is often at a 'G' value < 1.0. Thus, this plot is often most useful for lower fluid loss cases.

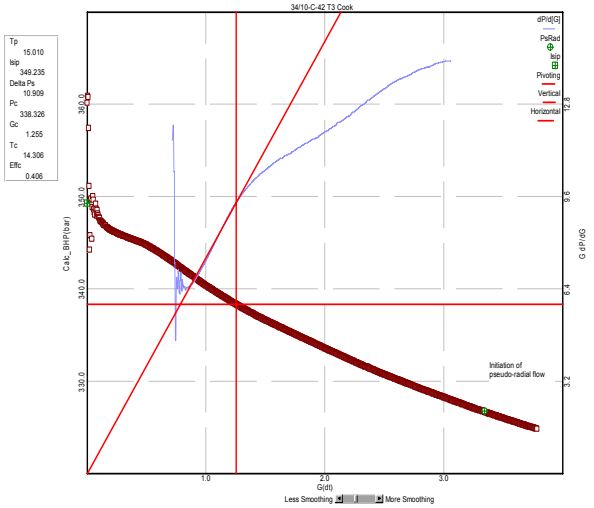

Fig. 11–G-dP/dG Plot of gel mini-frac in Gullfaks Well C-42T3.

Finally, and after picking closure stress, "net fracturing pressures" during injection (corrected for near wellbore friction/tortuosity) should be matched by application of a P-3D or 3D frac model which fully couples fluid flow with rock mechanics. Also, the same model must match the pressure decline rate for Phase I (time to closure) or "fluid efficiency". "Fluid efficiency "is defined as the ratio of the fracture volume to the total volume pumped at the end of pumping. For a relatively simple case where gross fracture height is equal to the fluid loss (or pay) height fluid efficiency can be defined by the simple identity,

$$eff = \frac{w_{avg}}{w_{avg} + 3C\sqrt{t} + 2S_p} \qquad \ldots\ldots\ldots\ldots\ldots\ldots (8)$$

Thus, a match of the net pressure and time to fracture closure, as shown in **Fig. 12**, represents the match of the dynamic geo-mechanical formation system (including fracture volum) and, therefore, substantiates the choice of a correct stress test value.

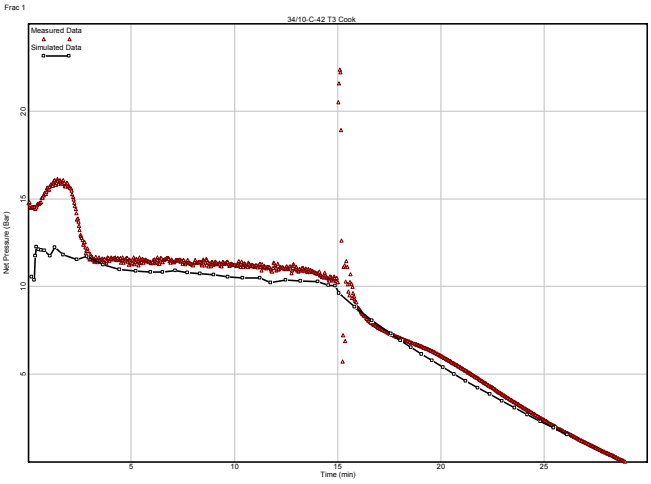

Fig. 12–Net Pressure match of gel mini-frac in Gullfaks Well C-42T3

Data Quality and Reliability

All "measured" (analyzed) stress data, gathered from permanent downhole gages located 100 - 300 m TVD (330 – 1000 ft) above top perforations or wireline downhole gages outside the perforations, are corrected to top perforations in **Table-1**. Appurtenant pore pressures represent in most cases RFT measurements a few days prior to testing. These measurements were confirmed by readings on the permanent pressure downhole gages just prior to testing. The remaining pore pressure data represent wireline pressure recordings in conjunction with the stress tests.

Stress tests in these soft formations have never been "hampered" by significant near wellbore friction anomalies (tortuosity) as often reported from similar type of stress tests in stiffer formations and which may complicate the analysis of this type of tests. Also, considering 1) the availability of a comprehensive laboratory based rock mechanical data base for this field and 2) the fact that the stress test analysis procedure includes matching of "net pressure" (on the order of only 10 bar or 145 psi for these soft formations) and "fluid-efficiency" it can be stated that the accuracy of closure stress values assembled from stress test analyses in the Gullfaks Field should be within 2 bar (29 psi).

Data Analysis

The closure stress data from all validated single zone mini frac tests in the Gullfaks Field are tabulated in **Table-1** and plottet in **Fig, 13.** Estimated original stress values are based on application of one γ-factor, as defined by the identity,

$$\Delta\sigma_x = \Delta\sigma_Y = \frac{1-2\nu}{1-\nu}(1-\beta)\Delta p = \gamma\Delta p \quad \text{..... A-9.}$$

"γ" equals 0.75 as suggested from "best fit" regression analysis of coherent data points from two wells – each containing three tests in the same formation, **Fig. 14** and **Fig. 15**. Three stress tests were undertaken at three different times (August 2003, September 2003 and April 2004), perforation intervals and reservoir pressures in well B-7A. This horizontal well was drilled with constant azimuth (106 degrees) approximately parallel to maximum horizontal stress (+/- 110 degrees) through the uniform, very unconsolidated and highly porous Rannoch Formation. Linear regression reveals best fit for an introduced internal or local stress gradient of 0.11 bar/m (Table-2) for this oil bearing zone by applying a γ-factor of 0.745, **Fig. 14**. Imposing an overall or average reservoir stress field gradient of approximately 0.209 bar/m (**Fig. 13**) would give a poorer correlation coefficient.

Likewise, three different stress tests were executed during an extended test sequence in three deep, separate and isolated Statfjord Formation water bearing zones in well B-40A which exhibited different reservoir pressures caused by uneven depletion. This latter well was drilled parallel to maximum horizontal stress and with an angle of 67 degrees through the pay. Regression shows best fit for an introduced internal stress gradient of 0.13 bar/m (Table-2) by using a γ-factor of 0.710. Again, imposing overall or average horizontal stress gradients of 0.209 or 0.310 bar/m, **Fig. 13**, would give worse statistical correlations. A lower γ-factor should, as discussed below, be expected for the deeper and more consolidated Statfjord Formation due to lower porosity, larger authigenic clay content and also a higher value of "β", ref. **Eq. A-9**.

Well	Formation	Top perf. TVDMSL	"Measured" (Bar)	Original stress (Bar)	ΔPp (Bar)
A-11	Rannoch	1988.3	378.7	399.0	27.0
A-12	Rannoch	1967.1	372.0	397.5	34.0
A-15	Rannoch	2038.2	397.5	419.6	29.4
A-35	Rannoch	1872.0	327.0	360.8	45.0
A-36	Rannoch	1754.8	319.8	340.8	28.0
A-37	Cook	1792.3	296.1	352.4	75.0
A-40	Cook I1	1751.9	296.2	326.2	40.0
A-40	Rannoch I1	1747.6	335.9	339.7	5.0
A-41B	Rannoch	1816.0	319.8	358.6	51.7
B-3A	Cook	1964.6	399.0	399.0	0.0
B-3A	Cook	1964.3	397.5	397.5	0.0
B-3A	Cook	1955.7	398.3	398.3	0.0
B-3A	Ness-3D	1900.3	337.8	367,1	39,0
B-07A	Rannoch	1745.8	320.3	321.8	2.0
B-07A	Rannoch	1745.2	311.5	322.0	14.0
B-07A	Rannoch	1742.8	285.0	321.8	49.0
B-12	Shetland/Shale	1918.0	387.5	387.5	0.0
B-19A	Rannoch	1841.3	335.6	352.9	23.0
B-20A	Cook	2044.0	380.8	379.7	-1.5
B-31	Drake/Rannoch	1794.3	333.7	333.7	0.0
B-31	Cook H3	1808.2	343.0	345.1	2.8
B-31	Drake/Cook H3	1830.0	342.0	342.0	0.0
B-32	Rannoch	1788.5	312.0	352.5	54.0
B-38	Cook I2A	1844.0	319.0	352.0	44.0
B-39B	Rannoch	1770.8	324.7	328.4	4.9
B-40A	Statfjord	2185.3	427.2	433.1	7.9
B-40A	Statfjord	2165.3	423.8	431.3	10.0
B-40A	Statfjord	2145.0	395.2	429.6	45.8
C-9A	Cook-2A	1950.4	331.0	366.4	47.2
C-9A	Cook-2C	1915.7	334.2	361.4	36.2
C-9A	Rannoch	1782.6	318.5	338.4	26.5
C-11	Rannoch	1863.0	324.5	344.8	27.0
C-11	Rannoch	1791.0	324.8	326.7	2.5
C-12	Rannoch	1837.7	308.0	336.5	38.0
C-12	Cook	1996.8	330.5	380.0	66.0
C-13	Statfjord	2038.6	368.5	387.6	25.5
C-22	Cook	1980.3	350.8	379.3	38.0
C-22	Rannoch	1844.4	333.9	348.2	19.0
C-23A	Cook	2046.7	365.7	377.0	15.0
C-23A	Ness/Shale	1874.5	347.5	347.5	0.0
C-24T2	Statfjord	1981.9	375.9	375.9	0.0
C-24T2	Statfjord	1940.5	344.0	357.9	18.5
C-26	Cook	2034.0	350.0	385.3	47.0
C-26	Rannoch	1887.2	327.8	349.8	29.3
C-28	Cook	1926.0	297.9	363.2	87.0
C-28	Rannoch	1779.7	313.7	338.5	33.0
C-35	Cook	1912.8	311.0	362.5	68.6
C-35	Rannoch	1772.4	297.0	341.3	59.0
C-40	Cook	1835.0	331.9	341.1	12.2
C-42T3	Cook	1864.5	338.3	353.3	20.0
C-45	Cook	1790.3	315.3	334.8	26.0

Table-1- Measured and depletion corrected closure stress values applying a γ - factor of 0.75 in the Gullfaks Field.

The poorer correlation coefficients by use of one overall horizontal stress gradient may suggest that there is no single "gross" horizontal stress gradient caused by tectonics through the reservoir structure, but several geo-mechanichally isolated segments with a normal Overburden dominated internal "local" stress gradient. Anyhow, there are several other reasons, as discussed below, why the stress field in the Gullfaks Field cannot be unique in the sense that all original stress values (prior to depletion) should fall on one common horizontal stress gradient across the field**:**

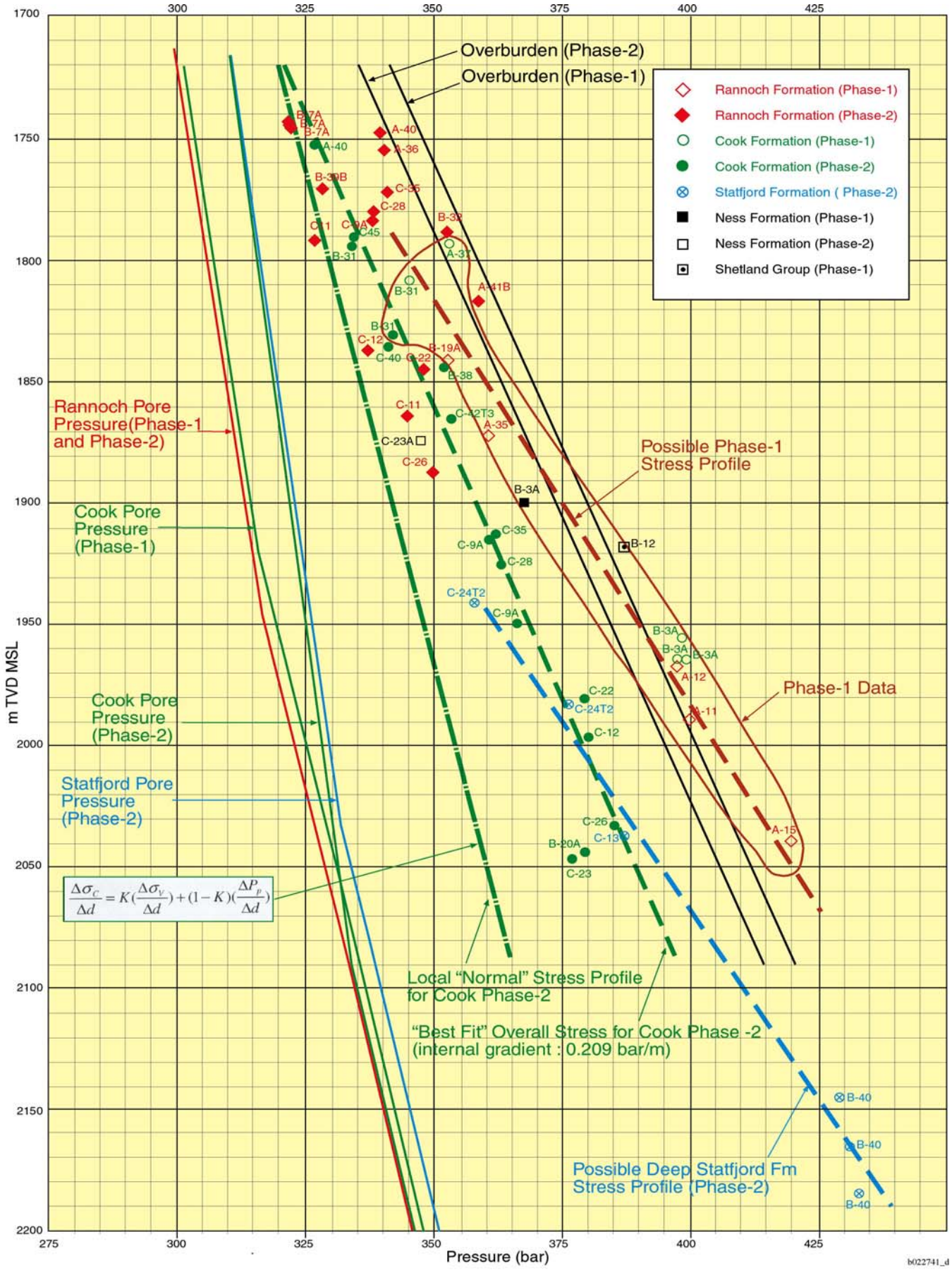

Fig. 13- Estimated original minimum horizontal stress, σ_x, versus depth

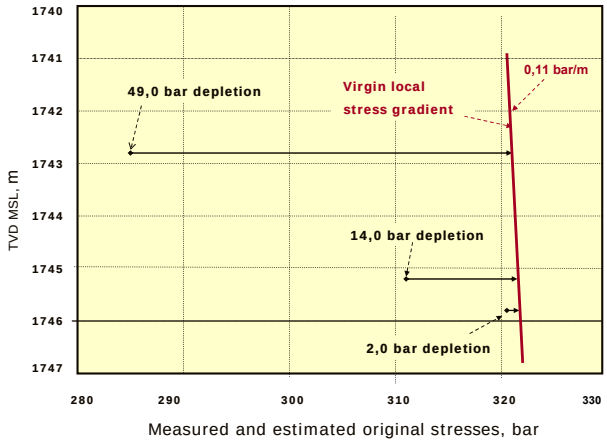

Fig. 14 – Regression based correction of measured stress values due to depletion in Gullfaks well B-7A.

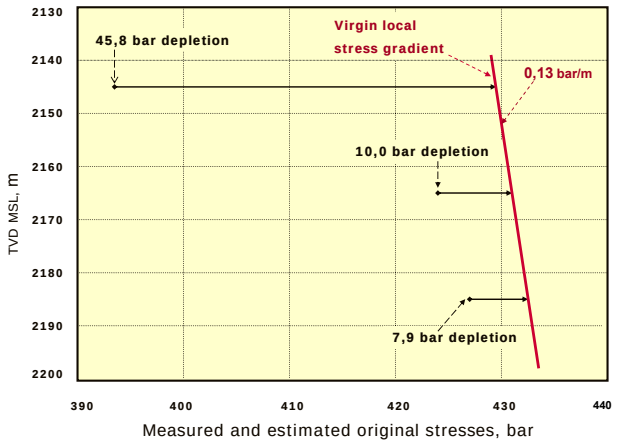

Fig. 15 – Regression based correction of measured stress values due to depletion in Gullfaks well B-40A.

Implications from Various Oil Water Contacts (OWC)

The reservoir pressures across the field in the water zone below the oil-water contacts are approximately equal **(**with a minor exception to the water zone in Statfjord Phase-2 Development**).** However, the reservoir pore pressures in the different formations at the same structural level are varying across the field owing to different oil-water contacts, **Fig. 13.** Hence, the original minimum horizontal stress (fracture closure pressure) gradient will vary slightly on account of its inherent dependency of pore pressure, **Eq. 9**.

$$\sigma_x = \sigma_C = \frac{\nu}{1-\nu}(\sigma_V - \alpha P_p) + \alpha P_p \quad \ldots\ldots\ldots\ldots\ldots (9)$$

Petrological Implications

A γ-factor of 0.75 suggests, according to **Eq. A-9**, a Poisson's ratio,ν, of 0.20, since "α" (=*1-C*$_r$*/C*$_b$), as defined in Appendix A, must be close to 1.0. A Poisson's ratio of 0.20 seems reasonable despite the wide scatter of data found for this parameter in the Gullfaks core laboratory database. Much of the laboratory data are of poor quality due to the unconsolidated nature of the core material. In laboratory analysis, cores taken from in-situ conditions to the laboratory will always be altered by the stress release due to the coring itself and also by other factors during transport, storage (freezing), cleaning and sample preparation. For mechanical properties, core alteration is most severe in the case of poorly consolidated materials. Further, the uni-axial testing procedure for determining both elastic moduli "ν" and "E" (Youngs's modul) is direct and easy. However, the accuracy is limited, in particular, with weakly consolidated and grained materials. Local inhomogenities in the cores or in the loading itself will have a strong influence on the results. Also, the radial deformation may be small compared to the grain size, which means that measurement of radial displacement at isolated points is a "crude" way to determine "ν". For instance, a Poisson's ratio of 0.1 means a radial displacement of approximately 20 μm which is less than the diameter of an individual sand grain. Thus, laboratory measurements cannot be made very accurate for estimating "ν" in unconsolidated formations as found in the Gullfaks Field.

Anyhow, the application of one unique γ-factor for the field as a total represents only a simplification to the correction of stress on account of pore pressure depletion. The parameters "α" and "ν" will probably exhibit different values for the Cook and Rannoch Formations due to significant variations in petrological and petrophysical properties. Also, these two parameters will probably vary within the same formation due to changing characteristics with stratigraphical depth, **Fig. 16**. Both formations are coarsing-upward sequences with highest porosity and permeability at the top.

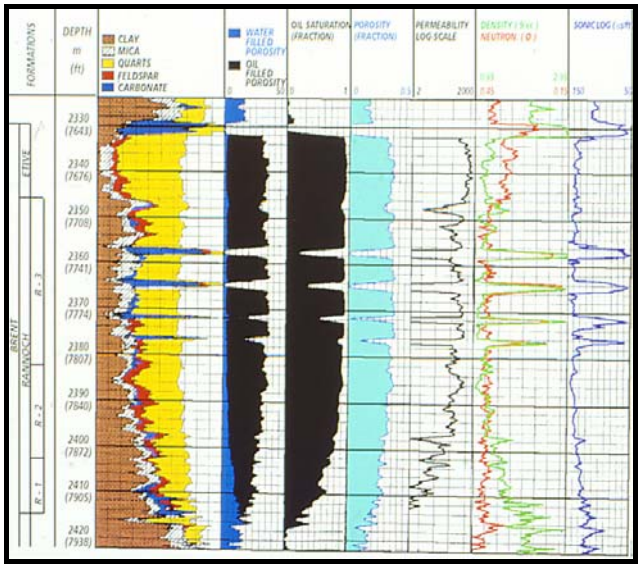

Fig. 16 – Log section of a typical coarsening upwards sequence in the Gullfaks Field: Rannoch Formation.

While the database indicates that "E" tends to decrease towards the upper Rannoch with highest permeability and least consolidation, "ν" shows no reliable trend in that respect. Old rock mechanical work, based on testing of various rock types with relatively low porosity, indicate relatively poor relationships between these two parameters[12]. However, these

findings under "static" and "dynamic" tests suggest that "E" increases with "ν". Also, later analysis of this work on a broad mixture of rock material indicates that both shear strength and rock compressive strength increases with Poisson' ratio[12]. Considering the nature of the Rannoch Formation one would expect the shear strength of the lower Rannoch to be significantly larger as compared to upper Rannoch; thus one should expect Poisson's ratio to be lower in Upper Rannoch.

Furthermore, acknowledged "old" borehole logging methods for sand strength calculations where based on an emperical relation, **Eq. 10**, between Poisson's ratio and shale content (and, thus indirectly, porosity) in shaly Gulf Coast sands, **Fig. 17**[13].

$$\nu = 0.124 I_{sh} + 0.27 \qquad \ldots\ldots\ldots\ldots\ldots\ldots\ldots\ldots (10)$$

The shale index[14] is defined as,

$$I_{sh} = \frac{\phi_S - \phi_D}{\phi_S} \qquad \ldots\ldots\ldots\ldots\ldots\ldots\ldots\ldots\ldots (11)$$

where ϕ_S and ϕ_D represent apparent sonic and density porosity, respectively. Thus, in theory, the γ-factor would gradually decrease towards the bottom of a coarsing upwards sequence sand body due to combined effects from potentially higher and lower values of "ν" and "α", respectively. The above relations

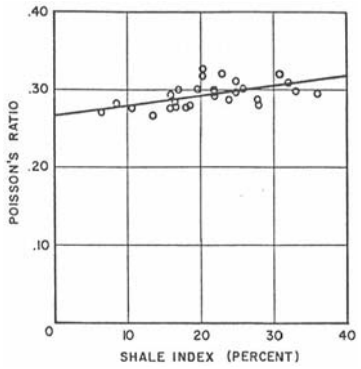

Fig. 17- Poisson's ratio versus shale index[13]

do not *quantitatively* match field testing results of unconsolidated sands in the Gullfaks Field (γ = 0.75) which according to **Fig. 18** suggest significantly lower values of "ν".

The limitations associated with laboratory static testing of such rock partly explain the scarcity of published data for very unconsolidated material. However, as mentioned in Appendix A and stated by others[15], there is a poorly documented understanding within the industry that unconsolidated sandstones with very high porosity (ø > 0.30) may have low Poisson's ratios (on the order of 0.15 or even less).

Application of state-of-the art sonic tools can measure both shear and compressional sonic velocities in extremely unconsolidated rock material. Thus, these tools may provide qualitative information about Poisson's ratio within the Rannoch and Cook Formation since the dynamic Poisson's ratio can be defined by the identity

$$\nu_{(dynamic)} = \frac{\frac{1}{2}\left(\frac{\Delta t_s}{\Delta t_p}\right)^2 - 1}{\left(\frac{\Delta t_s}{\Delta t_p}\right)^2 - 1} \qquad \ldots\ldots\ldots\ldots\ldots\ldots\ldots\ldots (12)$$

It remains questionable whether a study of this kind would be dependant on uncertain but significant corrections factors between static and dynamic rock mechanical parameters for this kind of unconsolidated rock. Anyhow, the application of one single γ-factor in **Table-1** and **Fig. 13** represents a trivial simplification to a complex rock mechanical scenario. Also, the fact that "α" may vary with time or act like a tensor in anisotropic rock, as briefly discussed in Appendix A, may further invalidate the simple approach since the data have been gathered over a period of 20 years. On the other hand, numerous pressure build-up data sets from the Gullfaks wells are consistently affected by tidal effects. Hence, it is believed that the immediate geo-mechanical response between the surface and the reservoir for this relatively shallow structure would eliminate concerns related to time effects. Also, this observation substantiates the application of overburden as a representative of vertical stress.

The general relationship, **Eq. A-9**, between petrological parameters and its impact on formation stress as a consequence of pore pressure variation is graphically presented in **Fig. 18**. A γ-factor of 0.75 corresponds to ν = 0.20 and α = 1.0 (or the combination of ν = 0.15 and α = 0.9).

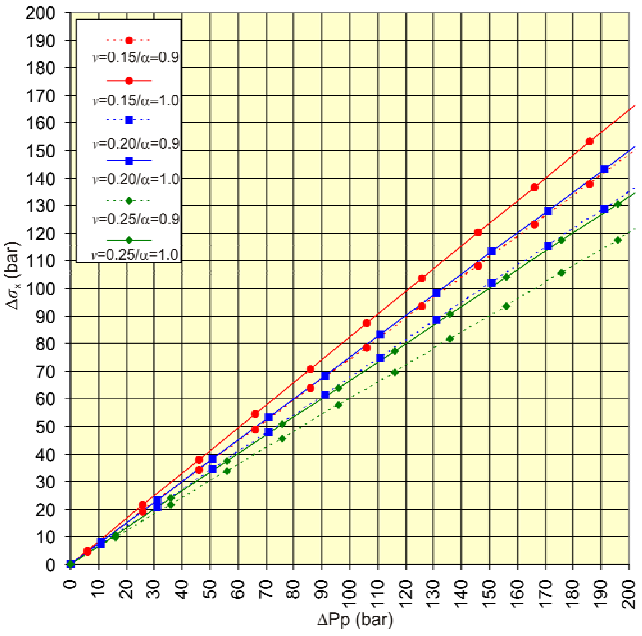

Fig. 18- Relationship between pore pressure change and minimum horizontal principal stress assuming uni-axial strain conditions.

Implications from Different Fluid Densities

Stress gradients are normally referred to in terms of total depth. However, "locally" within a formation, the "local" stress gradient can be (and probably generally is) different from the "gross" TVD stress gradient. Using **Eq. 13** (a conversion of **Eq. 9**) and assuming "α" equal to 1 (as

discussed in Appendix A) and K = ν/1- ν, a relationship between stress and depth can be written as

$$\frac{\Delta\sigma_C}{\Delta d} = K\left(\frac{\Delta\sigma_V}{\Delta d}\right) + (1-K)\left(\frac{\Delta P_p}{\Delta d}\right) \quad \ldots\ldots\ldots\ldots (13)$$

Further, assuming K = 0.25 (ν = 0.20) and $\Delta\sigma_V/\Delta d$ equal to the local "Overburden" gradient of 0.214 bar/m (0.945 psi/ft), **Fig. 13**, internal closure stress gradients, $\Delta\sigma_c/\Delta d$, can be tabulated, **Table-2**, as a function of different fluid densities or pore pressure gradients. Specific fluid density varys from of 0.6 to 1.034 s.g. in the Gullfaks Field. The local "Overburden" gradient is based on an average log derived bulk density of 2.15 g/cc through the reservoir. Hence, different formations containing hydrocarbons with slightly different fluid densities may have contributed to several uneven original "local" horizontal stress gradients across this field.

Fluid density (g/cc)	Pore pressure grad. bar/m (psi/ft)	Closure stress grad. bar/m (psi/ft)
0.60	0.060 (0.264)	0.098 (0.434)
0.70	0.070 (0.308)	0.106 (0.467)
0.80	0.080 (0.352)	0.113 (0.500)
1.034	0.103 (0.455)	0.131 (0.578)

Table-2- Internal gradients for different fluid densities.

Uneven Tectonic Impact

The data in **Fig. 13** strongly suggest that the major fault, **Fig. 19**, separating the western part of the field (Phase-1 Development) from the eastern horst complex (Phase-2 Development) is absorbing a major part ot the tectonic impact from NW-SE (apparent direction for maximum horizontal stress) set forth by the North Atlantic ridge. Thus this fault apparentely "divides" the field into two major and separate stress regimes. Comparing stress data for the Rannoch formation on both sides of this major fault which has the same OWC and identical fluid, petrophysical and rock mechanical parameters support this theory, **Fig. 13**. Also, inclusion of closure stress data for the Cook Formation (with a deeper OWC and, consequently, a relatively higher pore pressure) verifies an obvious change in effective closure stress ($\sigma_c - P_p$) across the subject fault at the same structural level, as illustrated in **Fig. 20**. The significant (≈ 50 percent) "loss" in effective stress in Cook Phase-2 (on the order of 23 bar (333 psi) at 1850 m TVD MSL), **Fig. 13**, can only be explained by less tectonic stress; the slight reduction in Overburden due to deeper water to the east above the field can only explain a small fraction of this reduction. Hence, the tectonic impact from NW-SE which appears to diminish towards the east across the field further complicates the overall field stress picture. Furthermore, the two regression lines, **Fig. 13**, indicating two separate horizontal stress gradients across the field of 0.30 bar/m (1.33 psi/ft) and 0.21 bar/m (0.93 psi/ft) for Phase-1 and Phase-2, respectively, strongly suggest larger tectonic influence with depth. Also, the apparent extraordinary overall stress gradient of the deeper Statfjord Formation in Phase-2, 0.31 bar/m (1.39 psi/ft), supports this theory. These remarkable stress gradients, which significantly deviate from

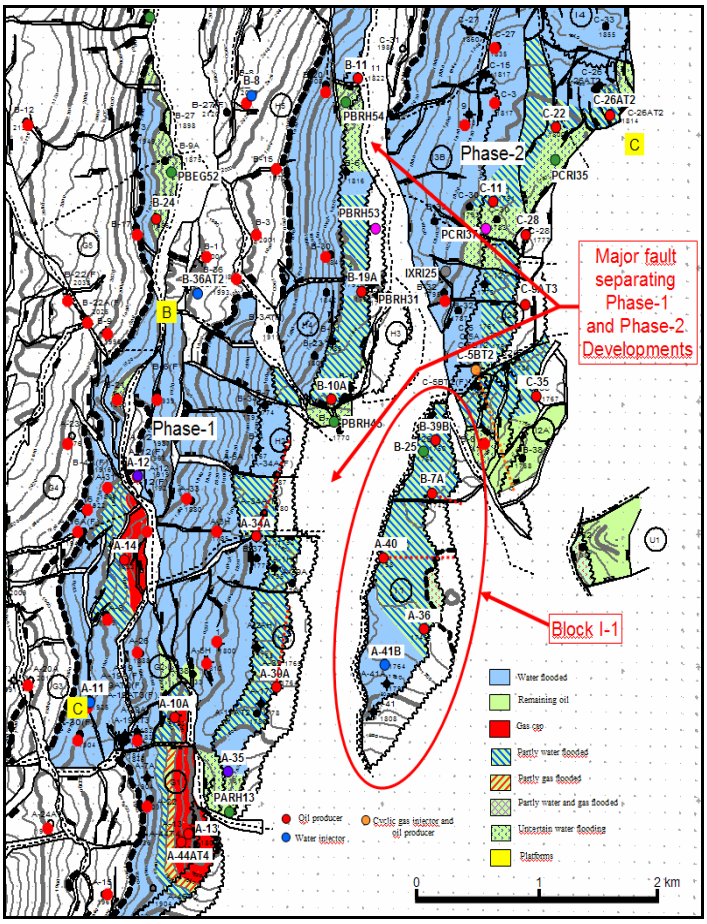

Fig. 19- Structual map of the top Rannoch Formation.

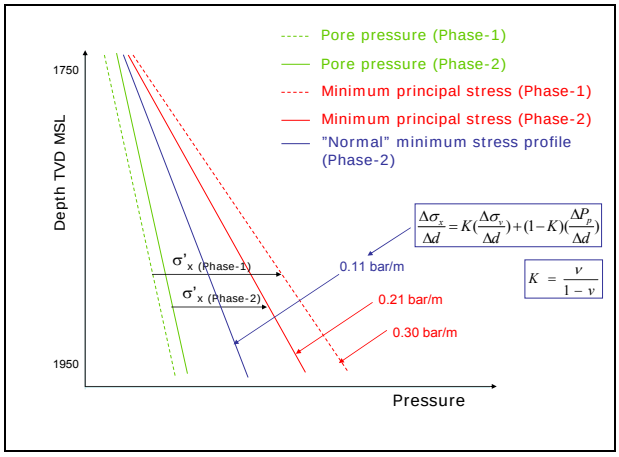

Fig. 20- Illustrative presentation of stresses revealing non-uniform tectonic impact with depth.

the theoretical local stress gradients in **Table-2**, indicate that the bottom of the Gullfaks structure may be in severe compression as compared to the crestal region of the field.

Eq. 9 is based on uni-axial strain condition. If the uni-axial strain assumption is relaxed and uniform (vs. depth) anisotropic tectonic strain is added, the elastic model becomes[16]

$$\sigma_x = \frac{\nu}{1-\nu}(\sigma_v - \alpha P_p) + \alpha P_p + \frac{E}{1-\nu^2}\varepsilon_x + \frac{E\nu}{1-\nu^2}\varepsilon_y \quad \ldots\ldots\ldots (14)$$

$$\sigma_y = \frac{\nu}{1-\nu}(\sigma_v - \alpha P_p) + \alpha P_p + \frac{E}{1-\nu^2}\varepsilon_y + \frac{E\nu}{1-\nu^2}\varepsilon_x \quad \ldots\ldots\ldots (15)$$

A dependency of stress on E is obtained, which means that the greater the E the greater the horizontal stress. This model can account for situations where sandstones are under higher stress than adjacent shales. The overburden is a principal stress but not necessarily the maximum principal one. **Fig. 13** reveals a difference of only 10 bar between pore pressure and minimum principal stress in the Cook Formation at the apex of the field at 1720 m TVD MSL east of the major fault dividing the Gullfaks Field into two apparent separate stress fields. The stress picture on an element of rock at this depth, **Fig. 21,** does not exclude the possibility of a virgin maximum horizontal stress on the order (or in excess) of Overburden. Unfortunately, lack of stress tests in this field with regard to determination of horizontal stress anisotropy makes this question open, although current "understanding" calls for a more normal stress picture where Overburden represents maximum principal stress at this depth**.** However, while Overburden apparentely represents maximum principal stress in Phase-2, apparent original minimum horizontal stress surpasses the calculated Overburden below 1950 m TVD MSL in Phase-1, **Fig. 13.** Hence the maximum horizontal stress

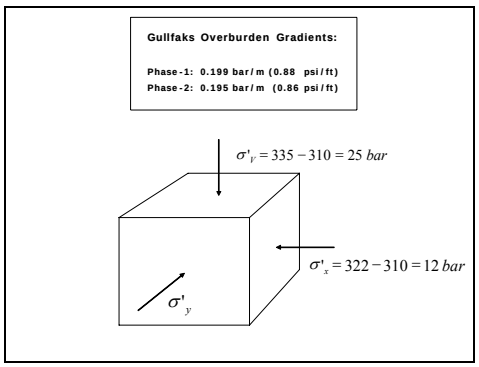

Fig. 21- Effective Stresses on an element of rock at the apex (1720 m TVD MSL) of the reservoir in the Gullfaks Field (Cook Formation – Phase-2 Development).

definitely represents the maximum principal stress below these depths. In view of the distinct lateral tectonic impact all the way from the apex towards the base of this field one may conclude that maximum horizontal stress represents the maximum principal stress at significantly shallower structural depths. This "observation" is not unique for the Viking Graben, **Fig. 1**; similar results are reported in conjunction with stress inversion studies of well data from the nearby Visund Field[17].

The distinct and increasing tectonic impact with depth can not be caused by an increase in Young's modul or change of any other relevant rock mechanical parameter with depth. The rocks in the Gullfaks Field show very little chemical compaction (dissolution and cementation) because of its shallow structural location. Thus, the depth dependant tectonic influence must reflect a yet unmapped regional tectonic pattern.

Also, there is evidence of a more complex stress situation caused by local "trapped" structural or tectonic disturbances caused by faults of different sizes and orientations. Stress tests in all Rannoch producers and one Rannoch injector in a mapped isolated reservoir segment (Block I-1), **Fig. 19**, strongly indicate that the stresses in this field are affected by local faults. Reservoir monitoring proves that there is poor pressure communication between the southern injector, B-41B, and wells B-7A and B-39A in the northern corner which must be caused by an obscure west-east tranmissibilty barrier (fault system) between wells A-40 and B-7A, **Fig. 19.** This observation is in coherence with the observed stress picture for this block which reveals a distinct and abrupt gap in stress data across this geographical area, **Fig. 13,** and **Fig. 22.** Minimum principal stresses for the wells in the northern region fall on one common stress gradient while the southern wells (A-36 and A-40) south of the transmissibility barrier or fault system belong to a 17 bar higher stress regime. Corrected and original stress in well A-41B, further south, deeper on the structure and close to a major fault, is even higher but in compliance with the understanding of increased tectonic impacts towards the major fault system south of the field where the reservoirs step down to the deeper Gullfaks Sør Field. In short, it appears that nearby fault activity has both increased stresses and caused stress relaxation in this field. Also, the higher stress in well A-41B is compliant with increased tectonic impact with depth**,** **Figs. 13** and **20.** This local stress anomaly, together with the

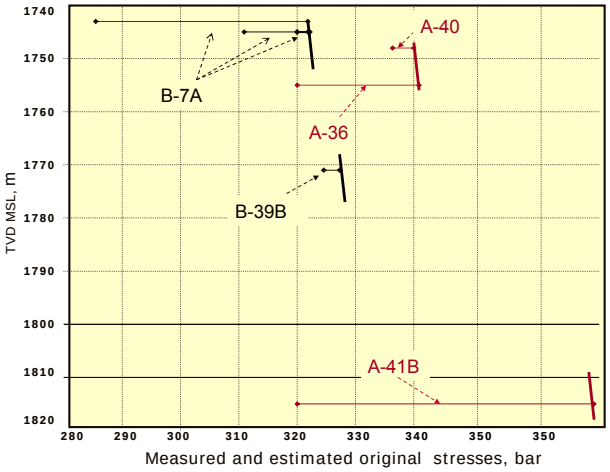

Fig. 22- Stress plot for Rannoch wells in Block I-1.

observed poor transmissibility across this area, entailed to the placement of a west-east fault across this block which is hard to detect from the relatively poor seismic data alone. Worth noting, the observed lower stresses in the northern corner of this block caused cancellation of a side-track drilling program for well B-7A due to prognozed too low formation strength values.

In summary, the virgin stress field in Gullfaks may therefore have looked like a "tangle" of individual stress gradients where "offset" in data may be explained by

- different OWCs,
- different rock mechanical parametes (α and ν),
- different fluid densities,
- diminishing tectonic impact (parallel to horizontal maximum stress) towards the east across the field,
- diminishing tectonic stress towards the north where the north-south faults pinches out,
- local increases in stress or stress relaxation due to nearby fault activity, and, finally
- additional compressional tectonic forces with depth**.**

Although the data in **Fig. 13** represent a substantial amount of information and values from a large geographical area, further mapping of stress in future wells to the west and north is imperative for an enhanced understanding of stress related rock mechanics in this mature field.

Implications from Poor Reservoir Communication

It has been questioned whether the measured higher stresses in the Phase-1 drainage area could be explained by less depletion dependant stress reduction due to confined or isolated small reservoir segments. As shown in Appendix A, it takes utmost small and unrealistic reservoir configurations, before the γ-factor becomes significantly affected by reservoir or depletion geometry. Aspects related to confined depletion, due to for instance extensive and sealing fault patterns and consequently poor reservoir transmissibility, do therefore not represent any significant uncertainty in this respect. Furthermore, 20 years of reservoir surveillance has confirmed extensive lateral reservoir communication across the field and none of the tested wells have been exposed to poor reservoir communication.

Aspects Related to (Elasto-Plastic) Deformation in the Gullfaks Field and Its Implication on Stress Path.

Fig. 23 shows rock compressibility data, "C_b", applied in reservoir modelling of compaction effects of reducing pore pressure from 310 to 260 bar (4557 to 3822 psi) in the Brent Group. The "flat" region around original pore pressure is

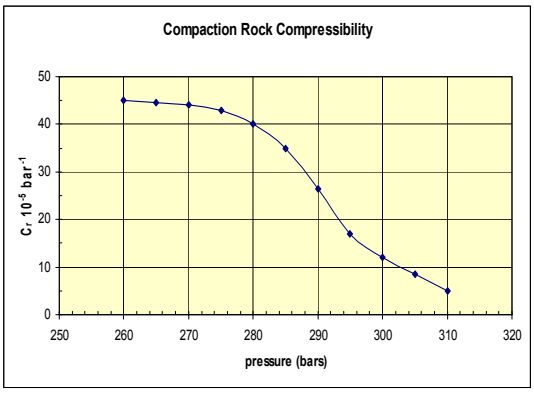

Fig. 23- Applied rock compressibility versus depletion in 3D reservoir modelling.

explained by an "inelastic" time lag between starting to produce the reservoir and occurrence of any significant degree of compaction[18, 19]. The remaining part of the "C_b" curve roughly corresponds to a normal stress-strain curve, as seen in **Fig. 24**. That is, a small region of "elastic" behavior, followed by the beginnings of failure and compaction, but with significant hardening (i.e., effective stress is continuing to increase), followed by what might be termed "plastic or elasto-plastic" deformation or compaction (where "C_b" can approximately be thought of as the slope of this stress-strain curve). An increase in pore pressure (due to water injection) will act to reduce the effective stress on the rock – i.e., we are essentially unloading the formation. **Fig. 24,** below, illustrates a typical stress-strain behavior for such cases, and while there is generally some hysteresis, in general most of the compaction is irreversible. That is, porosity lost during the

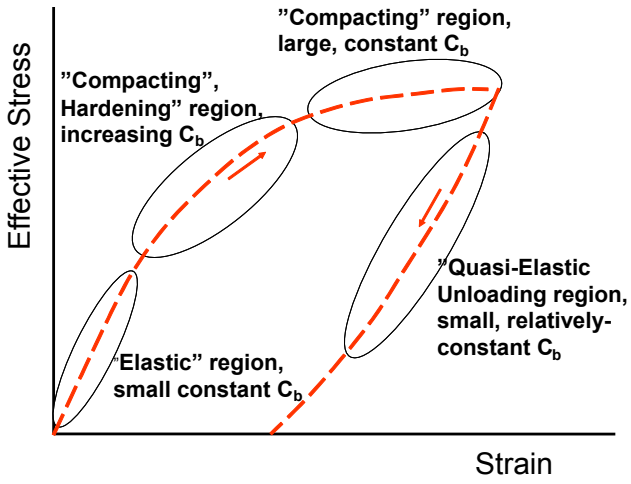

Fig. 24-Typical rock stress-strain curve during loading (i.e., reservoir pressure drawdown) and unloading (i.e., subsequent reservoir pressure increase from injection)

drawdown is not totally recovered as pore pressure is later increased[20]. The only mechanism for recovery of the porosity during injection would probably be if the increased pore pressure reduced the effective stresses to the point that the formation begins to undergo shear failure. This is normally a "dilatant" failure mechanism, and thus volume increases. This type of "failure mechanism" may probably result in gross formation failure, sand production, etc. Still, the relation of all this to how the minimum in situ stress changes with pore pressure is not specified simply by the C_b behavior above, or by a simple stress-strain relation. During the initial "elastic" behavior, the ratio of in situ stress change to reservoir pressure decrease is governed by "ν". This determines how much the rock would like to expand laterally for a given vertical compaction. Then, after failure/compaction begins, the vertical compaction to "desired lateral expansion" ratio is governed by the yield surface for the rock.

There is, based on **Fig. 13,** no evidence of elasto-plastic failure within the range of depletion evidenced in the unconsolidated sandstones formations which have been stress-tested in the Gullfaks Field. Minimum principal formation stress has not dropped like 1:1 with depletion (as discussed in Appendix B) in severely depleted wells in Gullfaks (C-28, A-37, C-35, etc.). Regression analyses of "depletion corrected" closure stress values in the Gullfaks Field suggest the ratio of stress change versus pore pressure depletion, γ, to be on the order of 0.75 for the most unconsolidated sands at the apex of the field.

Implications for Well Planning and Future Work

The overpressured nature and consequently low effective stresses found in the Gullfaks Field call for low drilling margins. Moreover, reservoir depletion narrows the margin between borehole collapse and loss of drilling mud (formation breakdown). Formation breakdown pressure can be calculated by the identity

$$P_{bd} = 3\sigma'_{\min} - \sigma'_{\max} + P_p + T \quad \ldots\ldots\ldots\ldots\ldots\ldots\ldots\ldots\ldots\ldots (16)$$

where σ'_{min} and σ'_{max} represent the minimum and maximum effective stresses acting perpendicular to wellbore. The equation is only valid for a non-penetrating fluid acting on a smooth, circumferential open borehole wall (with no natural or drilling induced fractures) which behaves in accordance with liner elastic theory. **Eq. 16** is valid for a vertical hole, or more precisely, a borehole which is parallel with one (any one) of the in-situ principal stresses. Thus, **Eq. 16** is valid for a horizontal well if the wellbore parallels either the maximum or the minimum in situ horizontal stress. For a vertical well in a reservoir where stresses change with depletion in acoordance with **Eq. A-9** or **Fig. 18** it can be shown that formation breakdown pressure will change in accoordance with appurtenant values in **Fig. 25**. Thus it can be shown that γ_f in **Eq. 17** is 0.5 for a vertical well if "γ" is 0.75.

$$\Delta P_{bd} = \gamma_f \Delta P_p \quad \ldots\ldots\ldots\ldots\ldots\ldots\ldots\ldots\ldots\ldots\ldots\ldots (17)$$

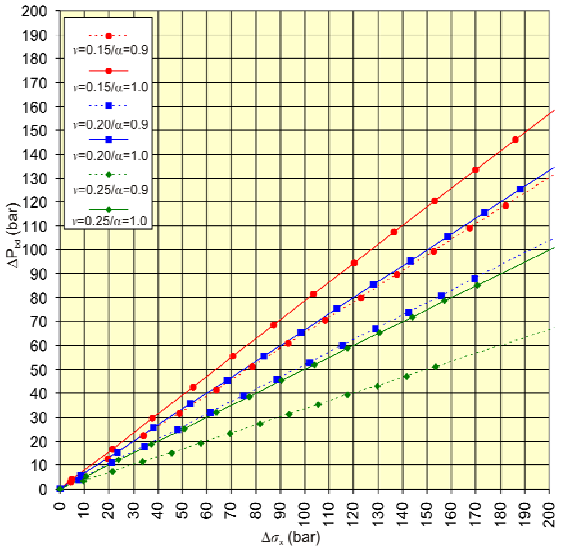

Fig. 25- Relationship between minimum horizontal principal stress and openhole formation breakdown pressure for a non-penetrating fluid in a vertical well.

A more careful or "conservative" approach has historically been used in conjunction with well planning in the Gullfaks Field in order to account for uncertainties related to deviated well and horizontal stress anisotropy effects. Formation breakdown pressure was set to minimum horizontal stress plus a constant (10 bar and 20 bar for relatively weak and strong rock, respectively). The γ-factor relating change in minimum horizontal stress to change in reservoir pressure was chosen to 0.7.

Finally recognizing the importance of large increases in effective stresses with depth and its implications on reservoir drillability, together with severe drilling problems caused by extensive lateral depletion (due to injection well maintenance problems), called for more accurate wellbore modeling in conjunction with well planning. The superposition of Kirsch's solution, the antiplane solution, and the solution for an internally pressurized borehole[21-23] which gives the solution for the stresses and the displacement around a perfectly circular well in a homogenious, isotropic, liner elastic medium, founded the basis for a computer program. The solution is based on the assumption of an "ideal" borehole wall with no pre-existing natural or drilling induced fractures. The program calculates formation breakdown pressure or borehole tensile failure when the minor effective principal stress reaches the tensile strength of the medium[24]. Formation breakdown pressure is "framed" since the program calculates this parameter for both "non-penetrating fluids" (typically mud with an effective filter cake and no significant spurt loss) and "penetrating fluids" which leak off and locally increase pore pressure and thus reduce breakdown pressure[25]. Although Kirsch's solution gives too high values for formation breakdown pressure since wellbores in actual rocks are not "ideal" and most often do not exhibit linear elastic behaviour during failure[26-28], it should be noted that this solution should give reasonable prediction for γ_f since rock deformation in the Gullfaks Field as a result of depletion is a linear elastic process. The outcome from this work shows that the old and simple approach may, on many occasions, give reasonable estimates of formation breakdown pressure, but does not account for the dramatic impact on γ_f from well deviation and potentially horizontal stress anisotropy and depletion. This program reveals that γ_f can be approximately "0" for deviated wells with azimuth perpendicular to maximum horizontal stress for small depletion scenarios in case of anisotropic horizontal stress and as large as 1.3 for horizontal wells which parallels maximum horizontal stress. **Figs. 26** shows results for well azimuth perpendicular to maximum stress and stress values (Overburden and original minimum horizontal stress

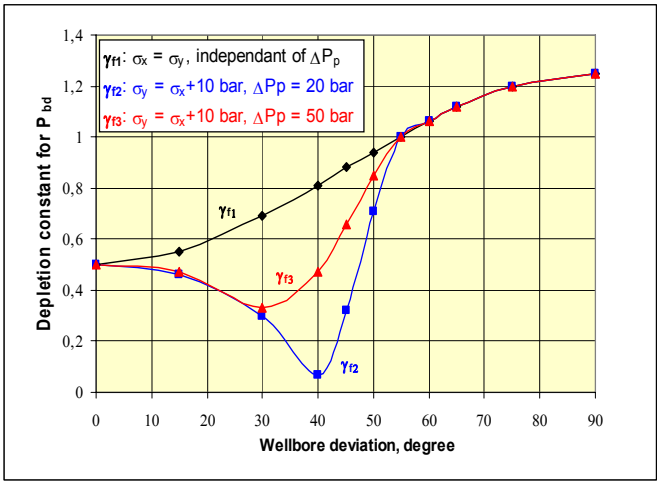

Fig. 26- Depletion constant, γ_f, for deviated wellbores drilled perpendicular to maximum stress at 1750 m TVD MSL (γ = 0.75).

equal to 348 bar and 330 bar, respectively) and original pore pressure (302.5 bar) at 1750 m TVD MSL in Phase-1.

The obvious tectonic stress component in the Gullfaks reservoirs calls for future mapping of maximum horizontal stress based on historical field drilling information and iteration of input by use of this advanced prediction tool. The revised and more accurate way of calculate formation strength for future wells also calls for continuous and more accurate mapping of formation minimum principal stress. Extensive mapping of local stress will contine and hopefully also entail to enhanced understanding of lateral stress variations, horizontal stress anisotropy and thus improved well planning.

Conclusions

1. The systematized stress data gathered in the Gullfaks Field over a 20 years development period and significant pore pressure variations (up to 87 bar or 1261 psi) exhibit geo-mechanical behaviour in coherence with linear elastic rock mechanical theory.
2. Field test results from very unconsolidated sands indicate that the γ-factor (relating change in minimum horizontal stress to change in reservoir pressure) is approximately 0.75. Thus, a Poisson's ratio of 0.2 represents an upper bound value (assuming uni-axial strain equations and α = 1.0) for these formations in this field.
3. The significant increase in effective horizontal stresses with depth has an important impact on formation integrity, drillability and thus well planning in this over-pressured reservoir. Apparent original minimum horizontal stress exceeds Overburden below 1950 m TVD MSL in the western part (Phase-1 Development) of the field. Maximum horizontal stress probably represents the maximum principal stress at significantly shallower structural depths.
4. Stress variations over small geographical areas are caused by subseismic faults. Knowledge of local stress variations is crucial in conjunction with well planning.
5. The tectonic impact is reduced towards the eastern margin of the structure.
6. Minor stress anomalies in this field cannot be occasioned by limited reservoir transmissibility or isolated small reservoir segments (localized depletion).
7. Accurate wellbore modeling which calculates the γ_f-factor (relating change in formation breakdown pressure to change in reservoir pressure) as a function of wellbore deviation (and azimuth and depletion in case of horizontal stress anisotropy) represents an important aid in conjunction with well planning.

Nomenclature

C_b = bulk compressibility, bar^{-1} (psi^{-1})
C_f = fracture compressibility, bar^{-1} (psi^{-1})
C_L = fluid loss coeffisent, ft/√minute
C_r = grain compressibility, bar^{-1} (psi^{-1})
C_t = total (system) compressibility, bar^{-1} (psi^{-1})
E = Young's Modul, bar (psi)
H = fracture gross height, m (ft)
H_p = net pay height, m (ft)
k = permeability, md
L = fracture half-length, m (ft)
P = pressure, bar (psi)
P_{bd} = formation breakdown pressure, bar (psi)
P_{net} = net (fracturing) pressure, bar (psi)
$\overline{P_{net}}$ = average P_{net} inside the fracture, bar (psi)
P_p = pore pressure, bar (psi)
q = flow rate, Sm3/d (bpd)
S_p = spurt loss, gal/100 sq.ft
T = tensile strength, bar (psi)
t = time, minute
t_s = shut-in time, minute
Δt_s = shear wave arrival time, μsec/ft (μsec/m)
Δt_p = compressional wave arrival time, μsec/ft (μsec/m)
v_L = velocity, ft/min
w_{awg} = average fracture width, in (cm)
α = 1- β
α_T = linear coefficient for thermal expansion
β = C_r/C_b
σ_v = vertical total stress, bar (psi)
σ_x = minimum horizontal stress or fracture closure pressure (σ_c), bar (psi)
σ_y = maximum horizontal stress, bar (psi)
ε_x = strain in direction of minimum horizontal stress
ε_y = strain in direction of maximum horizontal stress
γ = $\Delta\sigma_x/\Delta P_p$
γ_f = $\Delta P_{bd}/\Delta P_p$
μ = viscosity, cp
ν = Poisson's ratio
ϕ = porosity, fraction

Acknowledgment

The authors would like to thank StatoilHydro and Petoro for permission to publish this paper.

References

1. Arthur Bale and Kjell Owren, Statoil A/S, and M.B. Smith, NSI Technologies Inc., "Propped Fracturing as a Tool for Sand Control and Reservir Management", SPE 24992, presented at the European Petroleum Conference held in Cannes, France, 16-18 November 1992.
2. Arthur Bale, Statoil, Michael B. Smith, NSI-Tech, Tony Settari, Simtech Consulting Services,Ltd: "Post-Frac Productivity Calculation for Complex Reservoir/Fracture Geometry", SPE 28919.
3. Fossen, H. & Hesthammer, J. 1998. Structural geology of the Gullfaks Field, northern North Sea. In: Structural geology in reservoir characterization (edited by Coward, M. P., Johnson, H. & Daltaban, T. S.).Geol.Soc.Spec.Publ.127,231-261.
4. Fossen, H., Odinsen, T., Færseth, R. B. & Gabrielsen, R. H. 2000. Detachments and low-angle faults in the northern North Sea rift system. In: Dynamics of the Norwegian margins (edited by Nøttvedt, A.) 167. Geological Society of London, Special Publications, 105-131.
5. Rouby, F., Fossen, H. & Cobbold, P. 1996. Extension, displacement, and block rotation in the larger Gullfaks area, northern North Sea: determined from map view restoration. *AAPG Bull.*80, 875-890.
6. Færseth, R. B., Knudsen, B.-E., Liljedahl, T., Midbøe, P. S. & Søderstrøm, B. 1997. Oblique rifting and sequential faulting in the Jurassic development of the northern North Sea. *J. Struct. Geol.***19**, 1285-1302.
7. "Seismically Determined Predrill Stresses for Improved Petroleum Production and Exploration", study by John K. Davidson, Predrill Stresses International, 2000.
8. "GERMAN-NORWEGIAN JOINT RESEARCH PROJECT ON BASIN ANALYSIS AND RESEARCH STUDIES-Project A2: Determination of stress trajectories in Northern Europe and the significance of stress field orientation for hydrocarbon production and local and regional tectonics", by Prof. Dr. Karl Fuchs and Dr. Holger Spann, Geophysical Institute, University of Karsruhe, September 13./14., 1990.
9. "Hydraulic Fracturing Manual", 2nd edition, 1992 NSI Techn. Inc.
10. SPE 25845, "A Systematic Method for Applying Fracturing Pressure Decline: Part 1", K.G. Nolte, M.G. Mack, and W. L. Lie, Dowell Schlumberger.

11. Barree, R.D. and Mukherjee, H.: "Determination of Pressure Dependant Leakoff and its Effects on Fracture Geometry" paper SPE 36424 presented at the 1996 SPE Annual Technical Conference and Exhibition, Denver, 6-9 October.
12. Kumar, J.: "The Effect of Poisson's Ratio on Rock Properties", SPE 6094, presented for the 51st Annual Fall Technical Conference and Exibition of the Society of Petroleum Engineers of AIME, held in New Orleans, Oct. 3-6, 1976.
13. Anderson, R.A., Ingram, D.S., and Zanier, A.M.: "Determining Fracture Pressure Gradients from Well Logs," JPT (Nov, 1973) 1259-68.
14. Alger, R.P. et al.:"Formation Density Log Applications in Liquid-Filled Holes," JPT (March 1963) 321-32; Trans., AIME, 228.
15. N. Morita and D.L. Whitfill, Conoco Inc., and O. Nygaard and A.Bale, Statoil A.S: "A Quick Method To Determine Subsidence, Reservoir Compaction, and In-Situ Stress Induced By Reservoir Depletion", SPE 17150, presented for the SPE Formation Damage Control Symposium held in Bakerfield, California, February 8-9,1988 and also Journal of Petroleum Technology, January 1989 (p 71 – 79).
16. M. J. Thiercelin, Schlumberger Cambridge Research and R. A. Plumb, Schlumberger-Doll Research,: "A Core-Based Prediction of Lithologic Stress Contrasts in East Texas Formations", SPE 21847, presented at the SPE Rocky Mountain Regional Meeting/Low Permeability Reservoirs Symposium, Denver, Colorado, USA (April 15-17, 1991), also in SPE Formation Evaluation (Desember 1994) pg. 251- 258.
17. D. Wiprut, M. Zoback, Department of Geophysics, Stanford University, Stanford, CA 94305-2215, USA.: "Constraining the stress tensor in the Visund field, Norwegian North Sea: Application to wellbore stability and sand production", International Journal of Rock Mechanics and Mining Sciences 37 (2000) 317-336.
18. L.P. DAKE, "Fundamentals of reservoir engineering", Elsevier-Scientific Publishing Company, 1978. p 101.
19. Merle, H.A., Kentie, C.J.P., van Opstal, G.H.C., and Schneider, G.M.G., "The Bachaquero Study – A Composite Analysis of the Behaviour of a Compaction Drive/Solution Gas Drive Reservoir". J.Pet.Tech. September 1976 pg.1107 – 1115.
20. Antonin (Tony) Settari and Dale A. Walters, Duke Engineering & Services (Canada) Inc.: "Advances in Coupled Geomechanical and Reservoir Modeling With Application to Reservoir Compaction", SPE 51927, presented at the 1999 SPE Reservoir Simulation Symposium held in Houston, Texas, 14 – 17 February 1999.
21. Deily, F. H., and Owens, T. C.: "Stress Around a Wellbore", SPE 2557, 1969
22. Bradley, W. B.: "Failure of Inclined Boreholes", J. Energy Res. Tech, Trans., AIME (Dec. 1979) 102, 232 – 239.
23. Richardson, R. M.: "Hydraulic Fracture in Arbitrarily Oriented Boreholes: an Analytic Solution", Proc., Workshop on Hydraulic Fracturing Stress Measurements, Monterey, California (Dec. 1981).
24. Daneshy, A. A.: "A Study of Inclined Hydraulic Fractures", SPEJ (April 1973) 61-68.
25. Haimson, B. E. and Fairhurst, C.: "Initiation and Extension of Hydraulic Fractures in Rocks", SPEJ (September 1967).
26. Y. Yang, M. B. Dusseault," Borehole Yield and Hydraulic Fracture Initiation in Poorly Consolidated Rock Strata – Part I. Impermeable Media", *Int. J. Rock. Mech. Min. Sci & Geomech. Abstr*. Vol. 28, No. 4, pp. 235 – 246, 1991.
27. Y. Yang, M. B. Dusseault," Borehole Yield and Hydraulic Fracture Initiation in Poorly Consolidated Rock Strata –Part II. Permeable Media", *Int. J. Rock. Mech. Min. Sci & Geomech. Abstr*. Vol. 28, No. 4, pp. 247 – 260, 1991
28. P. Horsrud, R. Risnes, R. K. Bratteli,: " Fracture Initiation Pressures in Permeable Poorly Consolidated Sands" ,*Int. J. Rock. Mech. Min. Sci & Geomech. Abstr*. Vol. 19, pp. 255 – 266, 1982..
29. Terzagi, K. van:"Die Berechnung der Durchlassigkeitsziffer des Tones aus dem Verlauf der Hydrodynamischen Spannungserscheinungen," Sber. Akad. Wiss., Wien (1923) 132, 105.
30. Biot, M. A.: " General Theory of Three-Dimensional Consolidation," J. Appl. Phys. (1941) 12, 155-164.
31. Handin, J., Hager, R.V. Jr., Friedman, M., and Feather, J.N.: "Experimental Deformation of Sedimentary Rocks Under Confining Pressure: Pore Pressure Tests," Bull., AAPG (1963) 47, 717-755.
32. Geertsma, J.: "The Effect of Fluid Pressure Decline on Volumetric Changes of Porous Rocks," Trans., AIME (1957) 210, 331-340
33. Michael J. Economides and Kenneth G. Nolte, "Reservoir Stimulation" Third Edition 2000, (3-9)
34. Perkins, T. K., and Gonzalez, J.A., "Changes in Earth Stresses Around a Wellbore Caused by Radially Symmetrical Pressure and Temperature Gradients," SPE 10080, 56th Annual Fall Meeting of SPE, San Antonio, Texas, October 5-7, 1981.
35. "Reservoir Compaction", Distinguished Author Series, A. Settari, SPE paper 76805
36. P.M.T.M. Schutjens, SPE, Shell/Sintef Petroleum Research; T.H. Hanssen, SPE, M.H.H. Hettema, SPE, and J. Merour, Statoil; P.de Bree and J.W.A. Coremans, Shell; and G. Helliesen, Norwegian Petroleum Directorate,: "Compaction-Induced Porosity/Permeability Reduction in Sandstone Reservoirs: Data and Model for Elasticity-Dominated Deformation", June 2004 SPE Reservoir Evaluation & Engineering, SPE paper 88441.
37. M. R. Norris, Dowell Schlumberger, B. A. Berntsen, L. Skartveit, C. Teesdale, Amoco Norway Oil Company: "Multiple Proppant Fracturing of Horizontal Wellbores in a Chalk Formation: Evolving the Process in the Valhall Field", SPE 50608, presented at the 1998 SPE European Petroleum Conference held in the Hague, The Netherlands, 20-22 October 1998.

Appendix A - Basic Elasticity Equations

Stress changes within consolidated rock which occur over a relatively short time period of months or years (relatively short compared to geologic time) due to changes in reservoir pressure can probably be predicted with reasonable accuracy assuming an elastic response of the rock to changes in stress, pore pressure, and/or temperature. For such an assumption, the basic relations between stress and strain (Hooke's Law of Elasticity) can be written as,

$$\varepsilon_x = \frac{1}{E}(\sigma_x - \upsilon(\sigma_y + \sigma_z)) - \alpha_T T \quad \ldots\ldots\ldots\ldots\ldots\ldots \text{(A-1)}$$

where ε_x is strain in the "x" direction, σ_x is stress parallel to the "x" direction, σ_y and σ_z are the stresses parallel to the "y" and "z"directions, E and ν are material constants the Young's modulus and Poisson's ration of the material, respectively, and $\alpha_T T$ is the coefficient of linear thermal expansion.

Also, two additional equations can be written for the strains in the "y" and "z" directions. However, two changes are required in this statement of Hooke's Law before applying elastic theory to a buried rock mass. First the basic equation, **Eq. A-1**, is written with "0" as a base point, e.g. assuming that all strains of the material can be predicted based on knowledge of the current state of total stress (and temperature). However, for a buried rock mass, an initial stress/strain state exists which has developed over long time periods in response to geologic/tectonic loadings, temperature and chemical changes, rock composition changes, etc which reflects anything but an elastic relation between historical stresses and strains. Therefore, the basic equations must be recast in the form of differences, e.g changes in stress/strain from the initial state can be predicted based on elasticity. Also, as first noted by Terzaghi[29] for soils, rocks and soils respond not to the total external loads, but to effective stresses, **Eq. A-2**, where some of the total external applied loads (e.g total stresses) are supported by the pore pressure of the rock/soil.

$$\sigma' = \sigma - p \quad \ldots\ldots\ldots\ldots\ldots\ldots\ldots\ldots \text{(A-2)}$$

Terzaghi's Law was modified by Biot[30] and later studied by Handin et al[31], **Eq. A-3**, by applying a correction factor, α, to the pore-pressure term, to account for the coupled diffusion/deformation process in elastic materials which corresponds to the change in pore pressure and accompanied variation in pore volume for consolidated formations. Also, petrologic aspects/parameters, as for instance cementation existing between the grains, may prevent the full magnitude of the pore pressure from counteracting the applied load. Hence, the overall mechanical response of the rock will be affected.

$$\sigma' = \sigma - \alpha p \quad \ldots\ldots\ldots\ldots\ldots\ldots\ldots\ldots \text{(A-3)}$$

In the ideal case where there is no porosity change under equal variation of pore pressure and confining pressure "α" can be expressed by the identity,

$$\alpha = 1 - \frac{K}{K_s} \quad \ldots\ldots\ldots\ldots\ldots\ldots\ldots\ldots \text{(A-4)}$$

where K and K_s represent the bulk modulus of the material and solid constituents, respectively. Further, **Eq. A-4,** can be expressed by the identity,

$$\alpha = 1 - \frac{c_r}{c_b} \quad \ldots\ldots\ldots\ldots\ldots\ldots\ldots\ldots \text{(A-5)}$$

as suggested by Geertsma[32], where C_r is the bulk compressibility of the grains (zero porosity) and C_b is the bulk compressibility of the rock/soil. Typically, for petroleum reservoirs, α is about 0.85 - 1.0, but its value changes over the life of the reservoir. Also, the poro-elastic constant, α, is a scalar only for isotropic materials. It is a tensor for anisotropic rocks[33].

Substituting the definition of effective stress, **Eq. A-3**, into the basic equation, **Eq. A-1**, gives

$$\Delta\varepsilon_x = \frac{1}{E}(\Delta\sigma'_x - \upsilon(\Delta\sigma'_y + \Delta\sigma'_z)) - \alpha_T \Delta T \ldots\ldots\ldots\ldots \text{(A-6)}$$

which can be expanded to the form below, **Eq. A-7**, where again two additional equations could be written for ε_x and ε_y.

$$\Delta\varepsilon_x = \frac{1}{E}(\Delta\sigma_x - \upsilon(\Delta\sigma_y + \Delta\sigma_z)) - \frac{1-2\nu}{E}(1-\beta)\Delta p - \alpha_t \Delta T \quad \ldots\ldots \text{(A-7)}$$

,where "β " is C_r/C_b. For soils or weekly consolidated sandstones as typically found in the North Sea and Gulf of Mexico, compressibility of the bulk, porous material is generally very large compared to the compressibility of quartz grains or solid constituents; thus "β" is small (< 0.05) and the effective stress parameter, "α", is near "1". Young's modulus, E, may vary from 13,6 Kbar (≈ 200 Kpsi) in high porosity, unconsolidated formations to 680 Kbar (≈ 10 Mpsi) in dolomite of low porosity and hard sandstones. Likewise, Poisson's ratio,ν, may have values from 0.15 in high porosity**,** unconsolidated formations to 0.3 in dolomite of low porosity and hard sandstones.

"Normal" Depletion

The primary interest of oil/gas applications in the above equations is the effect of changes on the pore pressure, Δp. Generally, a very large, relatively flat region is being depleted, that is a region whose lateral extent is much, much greater than its vertical thickness. As pore pressure in the zone is reduced, the rock tries to compact (e.g. negative Δεx, Δεy, Δεz) as predicted by the elasticity equations above. However, due to the large, lateral (top and bottom) surface areas which are connected to rock with no depletion - no lateral compaction is possible. Thus the compaction is in a purely vertical or "uniaxial" compaction mode. For such a case, $\Delta\varepsilon_x$ and $\Delta\varepsilon_y$ (the two lateral direction strains) are "0". Using this condition, $\Delta\varepsilon_x = \Delta\varepsilon_y = 0$, in the equations above, the change in the horizontal stresses within the depleted region can be computed by the identity,

$$\Delta\sigma_x = \Delta\sigma_Y = \frac{\nu}{1-\nu}\Delta\sigma_Z + \frac{1-2\nu}{1-\nu}(1-\beta)\Delta p + \frac{E}{1-\nu}\alpha_T \Delta T \ldots\ldots \text{(A-8)}$$

Since the vertical, total stress, σ_z, is typically taken to equal the weight of the overburden; $\Delta\sigma_z$ = "0". Also, for simple primary production depletion there is no changes in the reservoir temperature. Thus, the change in horizontal, total stresses are given by,

$$\Delta\sigma_x = \Delta\sigma_Y = \frac{1-2\nu}{1-\nu}(1-\beta)\Delta p = \gamma\Delta p \quad \ldots\ldots\ldots\ldots \text{(A-9)}$$

where "γ" typically has a value of 0.66. That is a 0.20 bar (3 psi) reduction in reservoir pressure causes a 0.14 bar (2 psi) reduction in the horizontal stresses. However, "γ" may theoretically vary from 0.5 in very hard rock to 0.8 in very soft rock depending on the values of "ν" and "β".

"Small Area" Depletion

A somewhat more complex case would consider what happens when the pore pressure is reduced in a region whose lateral extent is similar to, or less than the regional vertical thickness of the reservoir. Perkins[34] used a superposition of two classical thermal-elastic stress solutions (1: a change in temperature inside an infinitely long cylindrical region inside an infinite, elastic solid, and 2: a temperature change inside a "semi-infinite" cylindrical region inside an infinite elastic solid) to determine the change in stress inside a "disk" shaped region with an arbitrary ratio of radius (e.g. lateral extent) to thickness (e.g. vertical height). Considering a "disk" shaped reservoir with a radius equal to "a" and a vertical thickness equal to "H", **Fig. A-1,** and further assuming that the pore pressure in this region is reduced (or increased uniformly), the change in horizontal stress along the vertical centerline of the region will, according to the superposition solution presented by Perkins, be given by the identity,

$$\Delta\sigma_x = \Delta\sigma_Y = \gamma\Delta p\left(1 - \frac{1}{4}\left(\frac{n_1}{\sqrt{1+n_1^2}} + \frac{n_2}{\sqrt{1+n_2^2}}\right)\right) \ldots\ldots \textbf{(A-10)}$$

where

$$n_1 = \left(z + \frac{H}{2}\right) / a \;,\; n_2 = \left(\frac{H}{2} - z\right) / a \;,$$

"γ" is the material parameter described in **Eq. A-9**, and "z" is described in **Fig. A-1**.

Consider the case where "a" is very large and "z" equal to "0" (e.g. the very center of the cylindrical, disk shaped region). In such a case, n_1 and n_2 approximately equal "0", and the relationship between changes in pore pressure and changes

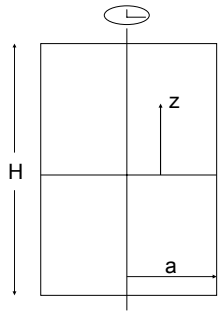

Fig. A-1 – "Disk" shaped reservoir model for stress change calculations inside reservoirs with limited extent.

in horizontal stress reduces to the simple uniaxial compaction case discussed above, **Eq. A-9**. Now consider a case where "a" is very small. For such a case, n_1 and n_2 become large, and $n_1/\sqrt{1+n_1^2}$ is approximately equal to "1". In this case, the relationship between horizontal stress and pore pressure reduces to

$$\Delta\sigma_x = \Delta\sigma_Y = \gamma\Delta p\left(\frac{1}{2}\right) \quad \text{(A-11)}$$

That is, the change in horizontal stress due to a pore pressure change in a region where the radius is much less than the thickness is "1/2" what the change would be for a case where pore pressure is changed over a large region (e.g. large laterally as compared to the region's thickness). The effect of "a/H" on pore pressure change induced stress changes (for 'z' equal to "0") is plotted in **Fig. A-2**. This shows that for a value of ("a"/"H/2") of about "4" (e.g. a drawdown area whose diameter is 4 times greater than its thickness), the change in stress is 88 % of what the change would be for a drawdown area which is infinite in lateral extent.

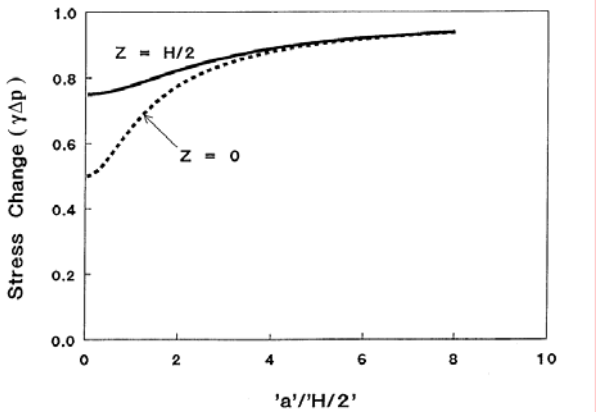

Fig. A-2 – Stress change versus reservoir configuration.

Appendix B - Aspects related to Elasto-Plastic Deformation

Eq. A-9 is based on elastic behavior and is certainly reasonably valid for many formations over a variety of conditions. However, for high porosity, "soft" formations, permanent compaction may occur indicating that the rock is undergoing some type of non-elastic deformation. How such deformation will affect the stress change will depend on the type of formation failure[35, 36].

Consider the idealized failure envelope in **Fig. B-1**. This plots "normal" stress (i.e., compressive, effective confining pressure) on the x-axis, and "shear" stress (i.e., maximum shear stress acting on the rock is ½ of the maximum in situ effective stress minus the minimum in situ effective stress) on the x-axis. As reservoir pressure is reduced, the stress on the formation will change as seen by the arrow, with the stress becoming more compressive, and the shear stress on the formation rock increasing. Eventually, this will lead to formation "failure" and some non-elastic deformation. What will happen at that point is determined by where the stress reaches the failure envelope.

On the "back side" (i.e., "Point 1"), at failure the rock faults and "dilates", i.e., a volume expansion occurs and the effective "γ" is related to the angle "θ". For an angle of 30° (typical of many clastic rocks), this "dilatant" or expansive behavior actually yields a "γ" of 0.66 – the same as seen for a Poisson's ratio value of 0.25 assuming α equal to 1.0. However, more generally the failure mode is on the "cap" of the failure envelop, in the "compacting" region. It is theoretically possible that the failure could be at the "top" of the envelope, "Point 2". In that case, the failure acts as an incompressible material, and effectively this gives a "plastic Poisson's ratio) of 0.5, and "γ" = 0.0. This has never been recorded in the literature, and thus is presumably a very rare occurrence – if, in practice, this ever happens.

More commonly, the failure is in the "compacting" region, in the neighborhood of "Point 3". In this type of failure, the rock actually loses volume, i.e., compacts, or porosity as the deformation occurs. The general trend for compacting behavior is to increase "γ". That is, there is less tendency for the rock to expand as it compacts vertically (since the rock is undergoing a volume reduction), the result is a very low value for "plastic Poisson's ratio", and "γ" is generally > 0.66. For the North Sea chalks, an effective "plastic Poisson's ratio" of "0" has been seen in multiple in situ stress measurements (as part of hydraulic fracturing operations[37]) – thus, "γ" is approximately "1". That is, horizontal stresses reduce 1:1 with reductions in reservoir pressure.

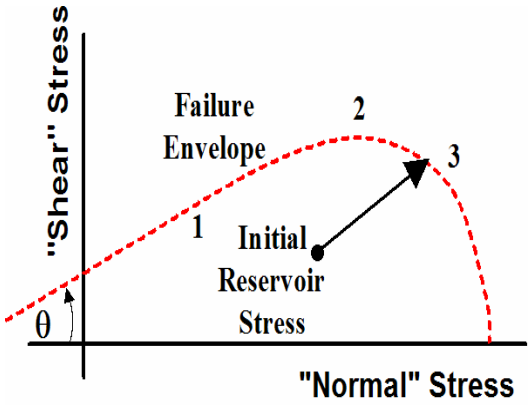

Fig. B-1 – Idealized failure envelope for compacting rock.